Automated Infrared Fiber Optic Characterizer

by

Chang Y. Lyu

Thesis submitted to the Faculty of the

Virginia Polytechnic Institute and State University

in partial fulfillment of the requirements for the degree of

Master of Science

in

Electrical Engineering

APPROVED:

Richard O. Claus, Chairman

Ronald J. Pieper

Ting-Chung Poon

July, 1989

Blacksburg, Virginia

Automated Infrared Fiber Optic Characterizer

by

Chang Y. Lyu

Richard O. Claus, Chairman

Electrical Engineering

(ABSTRACT)

Recent progress in reducing the extrinsic losses of fluorozirconate optical fibers has increased the material research efforts for these new waveguides. Fluorozirconate fibers, which are inherently more transparent than silica fibers, are predicted to have intrinsic losses as low as 0.001 dB/km at 3.45 μm [11]. Unfortunately, high intrinsic losses still plague these new optical fibers and these losses must be understood before ultra-low loss fibers become a reality. An automated fiber optic characterizer can help determine the loss mechanisms and the optical properties of fluorozirconate fibers so extrinsic loss mechanisms can be understood and eventually controlled. The automated fiber optic characterizer can also speed up the measurement process by using a microcomputer to align the fiber, calculate the results, and plot the graph. This thesis presents the technical issues involved in the design and construction of an automated infrared fiber optic characterizer. The thesis also outlines the test results of a constructed automated fiber optic characterizer. The characterizer measures spectral attenuation between 0.8 μm and 4 μm, differential modal attenuation between 1.6 μm and 4 μm, and numerical aperture at 1.55 μm and 2.55 μm.

Acknowledgements

Without the help of many people, I would have never completed this thesis. During my stay at Virginia Tech, I have learned much valuable information, as well as made some good friends.

I would like to especially thank my graduate advisor, Dr. R. O. Claus. His encouragement, patience, and assistance were greatly appreciated. R. G. May also deserves special thanks for his technical support and guidence.

Dr. R. Pieper's technical support and patience were important to me as well. Thanks also to T. C. Poon for being a member of my graduate committee.

Much credit must be given to B. Roarke. He spent many hours working on the software portion of this project, and his help was invaluable.

Thanks goes to L. J. Lu for his help with the mechanical design of the measurement system.

Without the technical support of Dr. P. Loveley and C. Sharr, this project would still be

unfinished. Many thanks to both of them.

I would like to especially thank my wife, for her help as well as her understanding, support, and love.

Table of Contents

List of Illustrations

1.0 Introduction

Current fiber optic technology is dominated by silica glass waveguides operating at the minimum attenuation wavelength of 1.5 μm or at a minimum dispersion limit of 1.3 μm [1]. Silica fibers have been fabricated with optical attenuation of 0.15 dB/km at a wavelength of 1.55um. This attenuation value is near the theoretical Rayleigh scattering limit. There are, however, optical materials which are intrinsically more transparent than silica. The heavy metal fluoride glasses, for example, are projected to possess minimum attenuation between 0.01 dB/km and 0.001 dB/km [2]. It is important to note that attenuation is only one of the physical properties of interest when selecting an optical fiber material. Other properties such as mechanical strength, chemical durability, aging, and drawing properties are also important in the selection of waveguide materials. Many research laboratories have chosen fluoride based glasses for waveguides because of favorable overall properties. Currently, short length (200 meters) step index fluorozirconate fibers suffer attenuation of 3 dB/km, far from their intrinsic value of 0.001 dB/km [3]. Many organizations, such as the Naval Research Laboratory, are exploring ways to reduce extrinsic loss. The large extrinsic attenuation value of step index fluoride fibers must first be understood and controlled before graded and dispersion shifted fibers fabricated using these materials are extensively produced and tested [2].

A fiber optic characterizer is an instrument that performs measurements of fiber parameters such as spectral attenuation, differential modal attenuation, and output far field. Quantitative evaluation of these fiber characteristics can aid the infrared material scientist study loss mechanisms in fluoride based fibers. Most laboratories that produce and characterize infrared fibers have manual bench top measuring systems which require extensive time to align and obtain data [4]. An automated fiber optic characterization system can speed up the measurement and characterization process by using a microcomputer to align the fiber, calculate the results, and plot the graph.

The Fiber and Electro-Optic Research Center at Virginia Tech is developing and constructing a computer controlled fiber characterization system that will measure certain parameters of fluorozirconate fibers. The system will measure spectral attenuation between the wavelength region of 0.8 μm and 4 μm; differential modal attenuation will be measured between the spectral region of 1.6 μm and 4 μm; numerical aperture will be measured at 1.55 μm and 2.55 μm.

This thesis presents the system requirements, design approach and component justification for the infrared fiber optic cable characterizer. A mathematical analysis of the measurements and a description of the optical devices involved with each measurement routine will be addressed. The accuracy and measurement repeatability of each measurement routine will also be tested on the constructed infrared fiber optic characterizer.

2.0 HEAVY METAL FLUORIDE FIBERS

The first fluoride glass was based on BeF_2 and originally synthesized 50 years ago. The fluoroberyllate glasses are difficult to handle because they are toxic and hygroscopic. The discovery of the heavy metal fluoride (HMF) glasses by Lucas and Poulain in 1974 opened the possibility of creating ultra-low loss fibers. The HMF glasses are less prone to crystallization and posses higher infrared transparency than the BeF_2 glasses. There are two categories of HMF glasses; the first type possess fluorozirconate (ZrF_4) or fluorohafnate (HfF_4) glasses as the network former, and the second category excludes ZrF_4 and HfF_4 but contain other metals and fluorides [5]. The AlF_3 - based HMF glasses are an example of the second category, which are not as stable as the fluorozirconate.

Extensive research has been conducted to produce high quality HMF fibers, like the fluorozirconates. A brief description of the glass preparation, the fiber fabrication and the loss mechanisms of ZrF_4 will be addressed in this chapter. Some applications of fluorozirconate fibers will also be presented.

2.1 Glass Composition and Synthesis

A stable glass structure is one of the most important parameters for an optical fiber material. Table 2.1 lists the material composition of some ZrF_4 based glasses, the most successful HMF fiber materials. The fluorozirconate glasses have ZrF_4 as the glass network former and BaF_2 is used as the primary network modifier. The addition of the metal fluorides of the rare-earths, alkalis or actinides stabilizes the glass. The most stable fluorozirconate glass contains four or more fluoride components. These stable glasses have a wide working range between 100° C and 150° C. The working range is defined as the difference between the crystallization temperature and the glass transition temperature. The fluorozirconates are compositionally flexible which is essential in producing fibers with compatible core and cladding [5].

Fluorozirconates may be one of the most stable HMF glasses but these materials must be cautiously handled. Contamination and defects introduced during the glass preparation process can adversely affect the optical properties of ZrF_4 fibers produced from these glasses [6]. Multi-component fluoride glasses have low viscosities at their liquidous temperature that cause the glass to form crystallized defects which scatter light. It is therefore essential to closely monitor fluoride glass at its liquidous temperature. It is also important to prepare HMF glass in highly controlled conditions because fluoride melts can react with certain crucible materials. This adverse reaction causes the glass to crystallize and/or produce defects. Platinum, gold or vitreous carbon is used as crucible material because these elements do not react with the fluoride glasses. Inert gases (N_2, Ar, He) or reactive gases (CCl, SF_6, HF, CF_4, BF_3) are used to remove water and other oxide

impurities from the melt [5].

2.2 Fluoride Fiber Fabrication

The preform and crucible techniques are the two main methods of producing fluoride based fibers. The preform method involves two steps. These steps are casting glass melts into fiber preforms and drawing preforms into fibers [7]. The crucible method as shown in Figure 1 is a continuous process of fiber fabrication, which does not require the separate production of a preform [9].

The built-in casting, rotational casting, and reactive vapor transport process are the three main techniques for preform fabrication. In the built-in casting method, shown in Figure 2, the cladding-glass melt is poured into a mold, which is heated to near the glass transition temperature. The mold is upset and the center portion of the melt spills out, leaving a hollow center, which allows the core glass to be cast. The entire structure is then annealed to produce a core-clad preform. Fiber lengths approaching 1 km have been produced with core diameters between 35 μm and 150 μm and overall diameter between 100 μm to 250 μm [5].

The rotational casting process is a modified built-in casting process that rapidly rotates the mold to achieve improved uniformity and core-cladding interface quality. The process, shown in Figure 3, starts with pouring glass melt into a gold coated cylindrical mold which

has been heated to the transitional temperature. The mold is then rapidly rotated to around 3000 rev/min or greater. The inner core material is then poured into the mold [5].

The reactive vapor transport technique involves the transport of a reactive mixture of vapors through a rotating fluoride tube. The reactive vapors are produced by low vapor metal halides or halogen gases. The refractive index of the core can be increased by adding Cl, Br, or I ions in the core region. The index profile of the resulting preform is paraboloid [5].

The continuous process of the crucible method is desirable because very long lengths of fiber can be fabricated. Fibers produced by this technique have higher optical losses than those produced using the preform method. The crucible method results in a higher incidence of devitrification and fiber distortion than the preform method because of the low viscosity of these glasses around the typical drawable temperature range [5].

2.3 Fiber Loss Mechanisms

The ultimate limitation of light propagation in fluoride based fibers is determined by the intrinsic loss mechanisms. The low power intrinsic losses determine the theoretical attenuation minimum of 0.001 dB/km as illustrated in Figure 4. These processes include bandgap absorption, Rayleigh scattering, self-phase modulation, nonlinear processes, and parametric processes. Only the low power intrinsic losses (bandgap absorption, Rayleigh

scattering) will be discussed [9].

Bandgap absorption occurs when sufficient photon energy absorbed into the valance band, which causes the electron to move across the forbidden band and into the conduction band. The forbidden bandgap determines the minimum photon energy required to move an electron from the valance to the conduction band [9].

Rayleigh scattering is the result of a localized fluctuation in the dielectric constant caused by density changes in the material. These material index fluctuations scatter light in all directions, causing power loss in the waveguide. The power loss is proportional to $1/(\text{wavelength})^4$ or $(\text{frequency})^4$. Higher frequency regions of the optical spectrum will experience more Rayleigh scattering than the lower frequency regions [9]. Iwasaki measured Rayleigh scattering of several fluoride based fibers using small lengths of fibers with low intrinsic scattering defects. The glass materials of these fibers are listed in Table 1. The $1/(\text{wavelength})^4$ dependence of Rayleigh scattering loss is well illustrated by his results in Figure 4. The ZBLYAL and ZOGA graphs in Figure 5 closely resemble the theoretical intrinsic losses. The ZBLYAN slope in Figure 5 is higher than that of silica, which is due to intrinsic and extrinsic scattering losses. The extrinsic losses are due to phase separation that causes strong scattering [10].

The extrinsic loss mechanisms must be controlled before the intrinsic loss of 0.001 dB/km of fluoride based fibers can be realized. Extrinsic losses are caused by electronic absorption from impurities or imperfections, vibrational impurities, surface absorption, macroscopic imperfections, and scattering impurities [9]. Electronic absorption can be caused by point defects, structural imperfections, and impurity atoms. Impurity atoms cause low energy absorption by creating states in the forbidden band. Impurity atoms can

be found in glasses or crystals. While point defects and structural imperfections are more common in crystals, rare-earth and transition metal ion impurities cause the most serious problems in fluoride based fibers, because their low-lying electronic configuration causes absorption in the near infrared region [9].

Impurities with vibrational characteristics that are infrared active can also cause serious attenuation problems. Some very common vibrational impurities are OH, H_2O, and O_2. Figure 6 illustrates the transmittance of H_2O as a function of wavelength. The specific absorption coefficient versus wavelength for various rare-earth and transition-metals is shown in Figure 7 [9].

The surface and core-cladding interface of the fiber each have a natural tendency to collect more impurities than the bulk material. This tendency will result in a higher attenuation and scattering loss for the surface and core-cladding interfaces. One approach to reducing the attenuation caused by surface defects is to increase the cladding diameter. A thick cladding diameter will reduce the interaction of energy between the evanescent field and the attenuating outer surface. This procedure is an effective technique because the evanescent field decays exponentially from the core-cladding interface [10].

Mie imperfection and structural imperfection scattering are two primary causes of extrinsic scattering losses in fluoride fibers. Mie scattering is dependent on 1/(wavelength)^2 while structural imperfection scattering is not wavelength dependent. Both losses are induced by imperfections that are as large or larger than the wavelength of operation. These imperfections can be crystallites, segregations, bubbles, impurity inclusions, and fluctuations at the core-cladding interface. Figure 8 shows that the transmission loss is linearly dependent on the defect density when operating at 2.55 μm. At approximately

2.55 μm the impurity losses due to absorption are small. Figure 8, therefore, reveals the significance of the scattering defects in fiber loss.

Figure 9 illustrates the wavelength independent scattering loss verses oxygen content in fluoride glass. These scattering mechanisms are caused by oxides formed in the melt before casting, when the double crucible method was incorporated. Oxides such as ZrO_2 and Al_2O_3 are created due to oxygen flow and water contamination of raw material during the drawing process [10].

Figure 10 illustrates the spectral attenuation of fiber produced by the Electrical Communication Laboratory of Japan. A minimum attenuation of 3 dB/km was obtained at 2.55 μm. The dominant loss mechanism for this fiber was the order of $1/(\text{wavelength})^2$ scattering which caused 2 dB/km. Impurity absorption contributed only 1 dB/km [10].

2.4 Applications of Fluorozirconates

The primary objective in developing fluorozirconate fibers is the possibility of long distance repeaterless telecommunication links. With the low intrinsic loss values of 0.01 dB/km at 2.55 μm would allow transmission links as long as 1500 km long. At present, we are far from the realization of 1500 km links due to extrinsic loss mechanisms and mechanical strengths of the fiber. The reported losses between 3 dB/km and 5 dB/km for 200 meter fibers provide other suitable applications. Fluorozirconate fibers can be used

in laser surgery, and fiber lasers. ZrF_4 fibers with high numerical aperture (0.2) and large core diameter (150 μm) have been used as waveguides for Er-Yag lasers. The resulting device has been successful in ablating tissue, arterial plaque and bone [3]. Fluoride glasses are important materials for rare earth doped laser hosts because they have higher radiative efficiencies than silicate glass. Fluorozirconate fiber lasers doped with Er^{3+} have been demonstrated to lase at 2.7 μm [37].

Glass		ZrF_4	BaF_2	GdF_3	LaF_3	AlF_3	YF_3	PbF_3	LiF	NaF	others
ZBGA[7]	core	60.5	31.7	3.8		4					
	cladding	58.6	30.7	3.7		7					
ZBLAYL[11]	core	49	25		3.5	2.5	2		18		
	cladding	48	23.5		2.5	3.5	2.5		20		
ZBLAN[10]	core	53	20		4	3				20	
	cladding	39.7	18		4	3				22	$13.3HfF_4$
ZBLAN[22]	core	54.9	17.65		3.92	3.73		4.90		14.71	$0.19InF_3$
	cladding	54.9	22.55		3.92	3.73				14.71	$0.19InF_3$

Table 2.1. Typical Fluoride Fiber Composition [10]

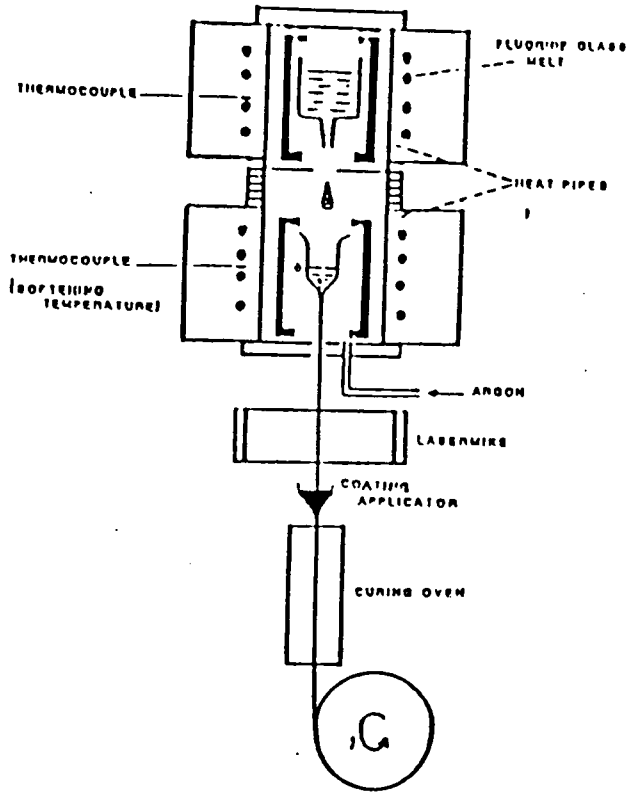

Figure 1. Crucible Approach for Fiber Drawing [2]

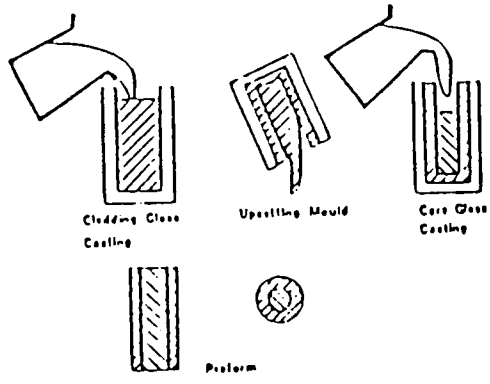

Figure 2. Sequence of Steps for the Built-In Casting Method [2]

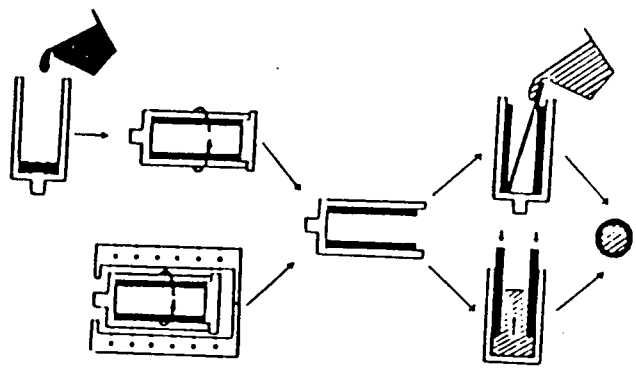

Figure 3. Sequence of Steps for the Rotational Casting Method [2]

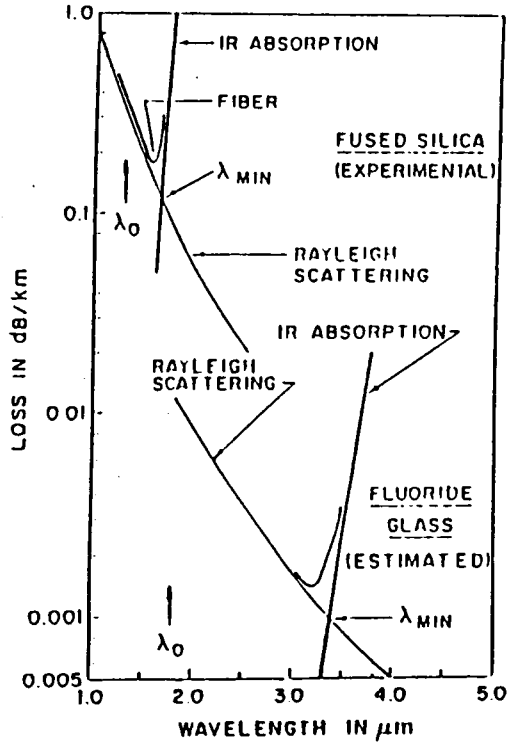

Figure 4. Theoretical Minimum Intrinsic Attenuation of Fluoride and Silica Fibers [11]

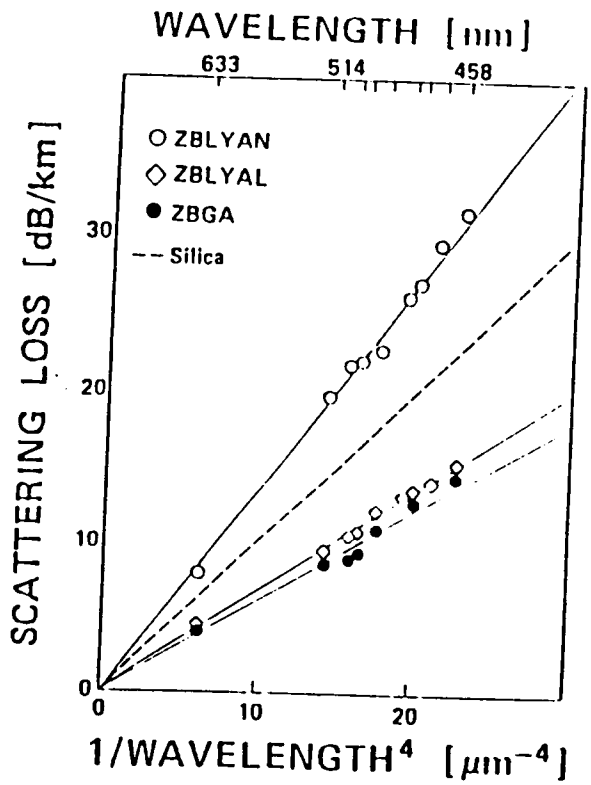

Figure 5. Wavelength Dependence of Scattering Losses [10]

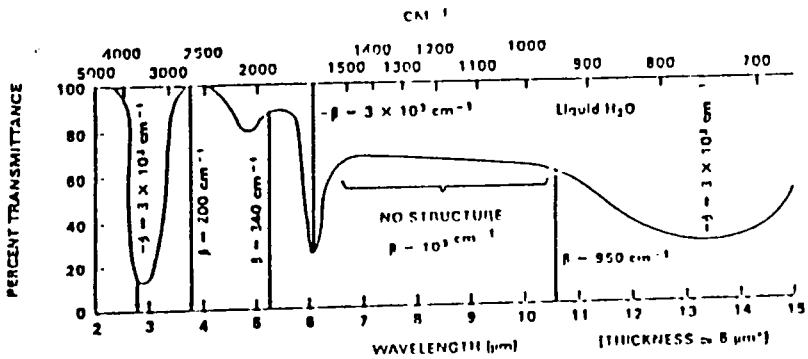

Figure 6. Transmittance of H_2O [9]

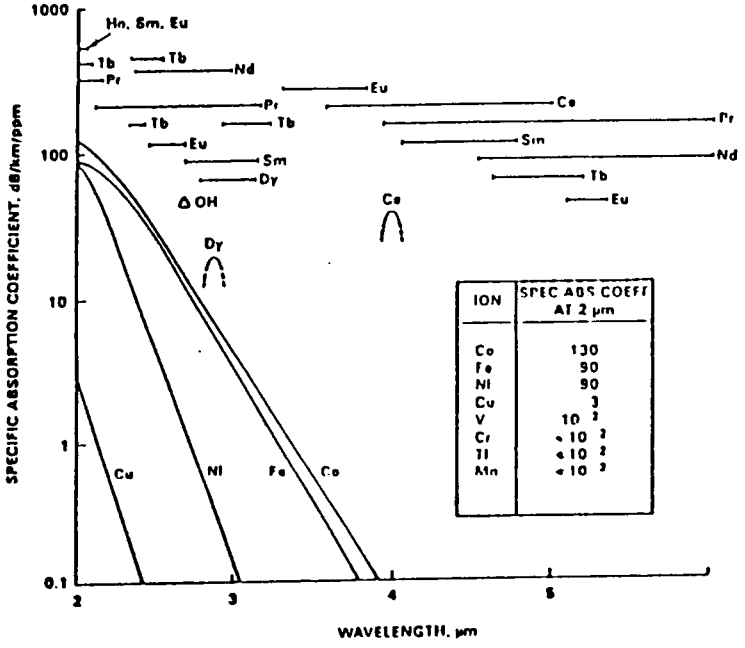

Figure 7. Absorption Coefficient of Rare-Earth and Transitional-Metal Absorption [7]

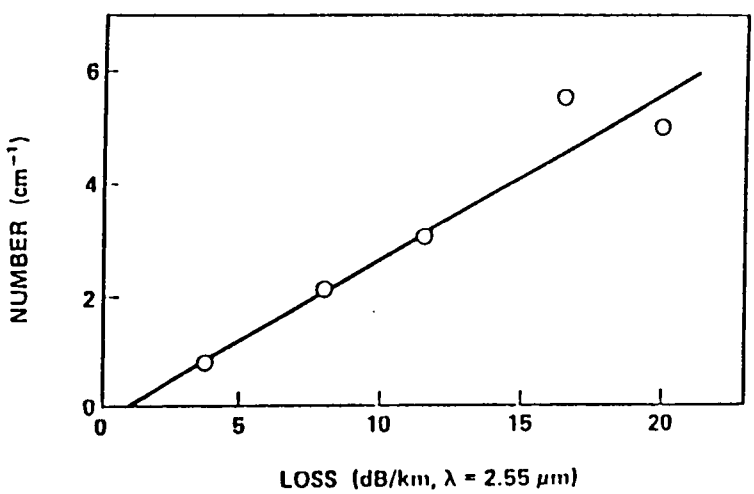

Figure 8. Transmission Loss at 2.55 μm with Scattering Defect Density [10]

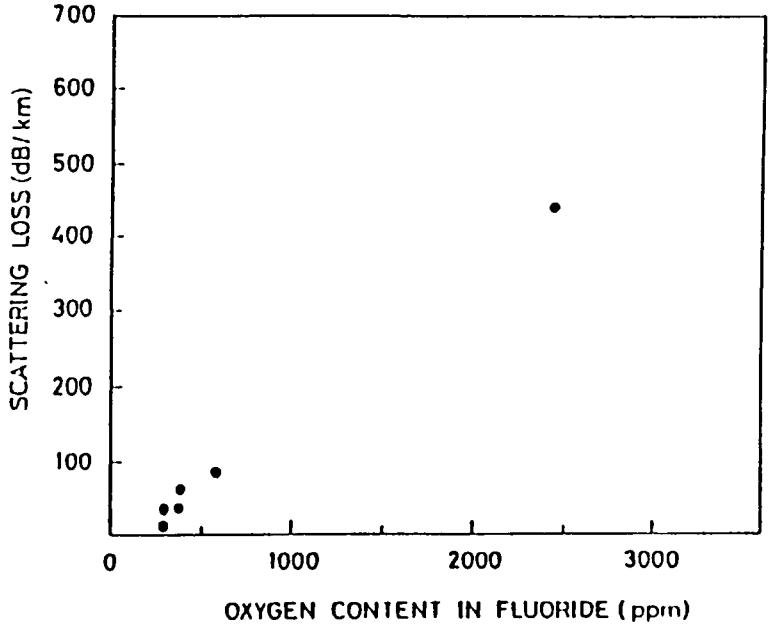

Figure 9. Wavelength Independent Scattering Loss and Oxygen Content [11]

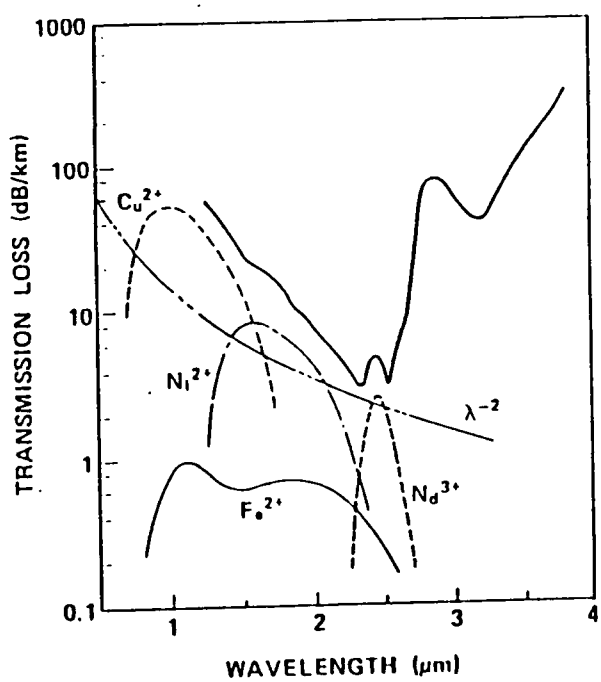

Figure 10. Spectral Loss of ZBLYAL Fiber [10]

3.0 System Requirements

Recent progress in reducing the attenuation of fluorozirconate fibers to 1 dB/km has increased the investigation of these materials [6]. To aid material research, a fiber optic characterizer is required to test the parameters of fibers produced. Currently, this test procedure is done manually, which requires much time. An automated characterization system, under the control of a microcomputer, can speed up the characterization process by automatically aligning the fiber, calculating the results, and plotting the graph. Naval Research Laboratory scientists are interested in obtaining an automated fiber optic characterization system which can be operated by a semi - skilled technician. The system must measure spectral attenuation, differential modal attenuation, and fiber numerical aperture. The system requirements of the infrared fiber optic cable characterizer will be discussed in this chapter.

3.1 Automated Alignment Requirements

The measurement system must have an automated pre-measurement alignment procedure, which will place the fiber ends at reference points on the optical bench. The input fiber

end's reference point will assure maximum power coupling into the fiber and provide consistent launch conditions for the test fiber. There are two ways for manually obtaining the reference point for the input/ output fiber ends. The two ways are by adjusting the fiber end images on a CID array camera or by using a pre-aligned input/output target pinhole. A detailed description of the system alignment procedure is presented in Chapter 5.

3.2 Spectral Attenuation Measurement Requirements

The system must perform spectral attenuation between the wavelength region of 0.6 μm and 4 μm with at least a 50 nm spectral resolution. The measurement equipment must accommodate 200 μm cladding diameter step index fluorozirconate fibers. An overfilled launch condition for 100 μm cores with the cladding modes stripped must be provided. The fiber optic characterizer should be automated so a microcomputer obtains the data and plots the loss measurement in dB/km verses wavelength. A detailed description of this measurement will be discussed in Chapter 5.

3.3 Differential Modal Attenuation Measurement Requirements

The measurement system must perform differential modal attenuation between the wavelength region of 1.6 μm and 4 μm with at least a 50 nm spectral resolution. A microcomputer should be used to obtain the measured data and plot loss in dB/km versus wavelength for a particular mode group excitation. A description of the DMA measurement using spatial filters and restrictive spot size is presented in Chapter 5.

3.4 Far field Radiation Measurement Requirements

Far field radiation measurements must be performed at 1.55 μm and 2.55 μm. An overfilled launch condition must be provided. A microcomputer must be used to plot the output fiber's far field pattern and calculate numerical aperture. This measurement will be performed using a linear far field scanner which will be discussed in more detail in Chapter 5.

4.0 COMPONENT SELECTION

Automated fiber optic cable characterizers for silica based fibers are commercially available. These systems perform measurements in the wavelength region between 0.6 μm and 1.5 μm. The Fiber and Electro-Optic Research Center (FEORC) currently owns a Photon Kinetics FOA-2000, an automated fiber optic characterizer. This measurement system can perform spectral attenuation in the wavelength region between 0.8 μm and 1.5 μm. It also measures far field, near field and pulse bandwidth [8]. The maximum implementation of system design and key components on the proven FOA-2000 for the design of an IR fiber characterizer has reduced the amount of research required for the design and production of the fiber optic characterizer. All key components of the FOA-2000 except for devices which cannot operate in the wavelength region between 0.6 μm and 4 μm. These components are the source, monochromator, lenses and detector. A discussion of the options and selection of these four devices will be presented in this chapter.

4.1 Source Consideration

The infrared fiber optic characterization system requires a source with stable high radiance output between 0.6 μm and 4 μm. The justification for the selection of an quartz-tungsten lamp is discussed in this section. A description of other incandescent and arc sources is also presented.

Arc and incandescent lamps are the two main types of infrared sources. The arc lamp operates at high pressure and radiates a thermal radiation continuum with sharp power peaks as shown in Figure 11. These lamps radiate most of the IR energy in the visible and ultraviolet region. The incandescent source emits its radiation by the thermal vibration of its filament molecules, and its spectral radiance is continuous. The spectral radiance of incandescent sources depend on the surface temperature and the emissivity of the radiator. The four most common incandescent sources are the blackbody, Globar (Silicon Carbide), Nernst Glower, and Tungsten [13].

Our fiber characterization system requires a smooth, continuous, powerful spectral irradiance from 0.6 μm through 4 μm. When using the cutback technique, accurate fiber measurements cannot be obtained with sharp variations in source power output [14]. The arc lamps are inappropriate for our fiber characterization system because of their sharp

power peaks. Only incandescent sources were further investigated

An ideal incandescent thermal source is the blackbody. An ideal blackbody absorbs all incident radiant energy; it is also the perfect radiator. A real source never exceeds the radiant output of a blackbody. Planck's law describes the spectral radiant emittance ($W \cdot cm^{-2} \cdot \mu m^{-1}$) at a given wavelength by the formula,

$$W_B = \frac{2\pi hc^2}{\lambda^5} \frac{1}{\left[e^{ch/\lambda kT} - 1\right]}, \tag{4.1.1}$$

where W_B is the spectral radiant emittance, λ is the wavelength, h is Planck's constant, c is the velocity of light in vacuum, k is Boltzmann's constant, and T is the absolute temperature [15]. Spectral radiance ($W \cdot m^{-2} \cdot \mu m^{-1} \cdot sr^{-1}$) is the radiant flux emitted per unit area and unit solid angle normal to the surface at a given wavelength. For perfectly diffuse sources, the spectral radiance (L) is given by the formula,

$$L = \frac{W}{\pi}, \tag{4.1.2}$$

where W is the spectral radiant emittance. A graph of a blackbody's spectral radiance verses wavelength is shown in Figure 12. Equation 4.1.1 describes an ideal blackbody while a factor called the emissivity can be used to describe incandescent sources that are not ideal. It is defined as,

$$\varepsilon = \frac{W_B}{W}, \tag{4.1.2}$$

where W is the spectral radiance of a non blackbody and W_B the spectral radiance of an ideal blackbody [12]. Emissivity is a function of material properties, wavelength of operation, and temperature of the emitter. An emissivity plot of Nernst Glower, Silicon Carbide (Glowbar), and Tungsten sources are shown in Figures 13, 14, and 15, respectively.

Commercially available blackbody sources approach theoretical limits with emissivity at approximately 0.99. These powerful sources operating above 2200 Kelvin would have been ideal for our system because they radiate more power than any other incandescent source at a particular temperatur. Unfortunately a 2200 Kelvin blackbody would cost approximately $13,000 and become more expensive with increased operating temperature. These sources are also extremely bulky and require special power supplies [18]. Spectral radiance plots a blackbody versus temperature is shown in Figure 12 [12].

A 2200 Kelvin Nernst Glower and controller can be purchased for approximately $4000. These sources are made from a combination of rare earth oxides and have a negative coefficient of resistance; therefore they must be preheated before a current can flow through the material. A Nernst Glower has a maximum operating temperature in air of 2200° Kelvin. The emissivity is approximately 0.3 between the operating range of 0.6 μm and 4 μm at 2200 Kelvin [17].

The spectral radiance of several incandescent sources, measured by K. Hardings, are shown in Figures 16. The Nernst Glower and low temperature SiC do not perform well between 1 μm and 4 μm as shown in Figure 16. The high temperature Tungsten and

Blackbody have the highest spectral radiance [17].

A Globar is a rod of silicon carbide typically 5 to 10 cm long and 0.5 cm in diameter. This source has an emissivity of approximately 0.85 in our wavelength of interest and has a usual operating temperature of only 1500 Kelvin. The spectral radiance cannot be large between 0.6 μm and 4 μm because of its low operating temperature [15].

A quartz-tungsten lamp is a widely used source in the visible and near infrared region because of its low cost and availability [13]. The current FOA-2000 fiber optic cable characterizer uses a quartz-tungsten lamp [8]. The filaments cannot function in air but operate well in a quartz envelope. Tungsten normally operates at temperatures of 3000°Kelvin and has an emissivity of 0.5 at 0.6 μm.and decreases to 0.15 at 4 μm. Tungsten has a good spectral radiance between 0.6 μm and 4 μm because of its high operating temperature [17].

The quartz envelope is usually the limiting factor when operating in the infrared region. Most quartz envelopes have poor transmittance at wavelengths longer than 2.5 μm, but the transparent quartz used in the Ushio®quartz halogen lamps have a transmittance of 90% between 0.6 μm and 4 μm [20]. A transmittance verses wavelength curve for quartz used in Ushio®bulbs is shown in Figure 17.

4.2 Monochromator

The monochromator for the IR fiber optic cable characterizer must effectively operate between the spectral region of 0.6 μm and 4 μm. Three gratings will be required to effectively cover this wide spectral region [21]. There are many single grating monochromators on the market but the three grating Jarrall Ash monochromator will be used for our system [21]. The three grating monochromator allows easier grating selection than the single grating monochromator because all three gratings are pre-aligned inside the monochromator. Some basic monochromator principles and terminology will be first addressed and the Jarrall Ash monochromator will be discussed.

A diffraction grating monochromator is a passive optical device which can select a narrow spectral bandwidth of radiation. The grating is usually made of a substrate with a large number of parallel grooves ruled in its surface and usually overcoated with aluminum. The grating, as shown in Figure 18, can have a sawtooth pattern. When parallel monochromatic light rays A and B areincident on adjacent grooves, there will be a path difference between their rays A' and B' as shown in Figure 18. The path difference is expressed as

$$a \cdot \sin(D) + a \cdot \sin(I), \qquad (4.2.1)$$

where a is the distance between the adjacent gratings and the angles D and I are shown in Figure 18. The summation of the rays A' and B' will result in destructive interference if the path difference is any odd multiple of half wavelength. Constructive interference will occur when the path difference is any integer multiple of wavelength. The basic grating equation for constructive interference can be expressed as

$$a \cdot (\text{Sin } D + \text{Sin } I) = m \cdot \lambda, \tag{4.2.2}$$

where m is an integer and λ the operating wavelength. We have only considered two grooves for the grating equation but adding more grooves only sharpens the peak of the sine square intensity distribution [12].

In a monochromator, the angle I and grating distance a are fixed values, while angle D is determined by rotating the grating. It is important to note that different orders of light will pass through the exit slit of the monochromator for different integer values of m. The monochromator will pass λ for the first order (m=1) and pass $\lambda/2$ for the second order (m=2) and so on. The first order has the highest power content and is the only desirable order. The higher orders (m >1) are blocked out by high wavelength pass filters [21].

The Jarall Ash Monospec® 27 monochromator can accommodate three separate gratings in a single monochromator as shown in Figure 19. The simultaneous mounting of the three gratings will easily allow the automation of the wavelength selection process. A stepper motor can easily be employed to switch the different gratings. To effectively cover the spectral region between 0.6 μm and 4 μm, three gratings will be used: 600 groove/mm blazed at 1 μm, 300 groove/mm blazed at 2 μm, and 150 groove/mm blazed at 4 μm. At the blazed wavelengths the individual gratings have the highest diffraction efficiency. The

600 groove/mm grating will operate between 0.6 μm and 1.79μm, while the 300 groove/mm will operate between 1.8 μm and 2.69μm. The 150 groove/mm will cover the spectral region between 2.7 μm and 4 μm . Each grating also has its own reciprocal linear dispersion value, which allows the calculation of spectral bandpass for a particular monochromator slit width. The reciprocal linear dispersion value is a function of wavelength but the variation is not significant for an individual grating. The average dispersion for the 600 groove/mm, 300 groove/mm, and 150 groove/mm gratings are 6 nm/mm, 12 nm/mm, and 24 nm/mm, respectively. The spectral bandpass for the 600 groove/mm, 300 groove/mm, and 150 groove/mm gratings will be approximately 3 nm, 6 nm, and 12 nm, respectively, when the slit size is 0.5 mm [21].

The monochromator wavelength selector will be automated with a stepper motor. The step angle on the motor is 1.8 degree per step, and it takes 200 steps for one complete revolution [22]. The Monospec® 27 has an analog wavelength counter which is calibrated to the 1200 groove/mm grating. To obtain the proper wavelength for each grating, the counter reading must be multiplied by 2, 4, and 8 for the 600 groove/mm , 300 groove/mm and 150 groove/mm gratings, respectively. One complete revolution on the wavelength selector corresponds to 25 nm of wavelength scan for a 1200 groove/mm grating. The gear ratio between the monochromator and stepper motor is 3:1. The number of steps on the motor required to scan 1 nm using the 1200 groove/mm grating can be calculated by the formula,

$$G \cdot \frac{N_m}{W_s}, \tag{4.2.3}$$

where N is the number of motor steps per revolution, W is the wavelength scan per revolution on selector, and G is the gear ratio between the monochromator and stepper

motor. Using equation 4.2.3, the 1200 groove / mm grating requires 24 steps for a 1 nm scan. The 600 groove / mm, 300 groove / mm, and 150 groove / mm gratings require 12 steps / nm, 6 steps / nm ,and 3 steps / nm, respectively [22].

4.3 LENS JUSTIFICATION

It is imperative that the lenses or mirrors on our measuring system introduce minimal loss. If significant loss is inherent in the mirror or lens, it will be difficult to launch adequate power into the test fiber. A minimum spot size of approximately 35 μm must also be achieved at the input end of the fiber to perform reliable differential modal attenuation measurements. Therefore our mirror or lens must experience minimal aberrations. It is also important to easily integrate our new optical components on the existing FOA-2000 to reduce the redesigning of key parts. This approach would allow us to most effectively utilize a proven working system. With these conditions in mind, the selection of spherical lenses over an off-axis paraboloidal mirror is justified in this section.

An off-axis paraboloidal mirror is a paraboloid covered with a coat of aluminum or gold. Gold has a reflectance of 97% from 0.6μm through 4μm as shown in Figure 20. This device will not experience spherical or chromatic aberration commonly associated with spherical lenses. Its image distortion is predominately due to surface quality. A blur spot of 35 μm can be achieved with an RMS surface irregularity of 126 nm. A mirror of this

quality will cost approximately $3000 [24].

The primary disadvantage of an off-axis paraboloidal mirror is the difficulty in implementing the mirrors on the current FOA-2000 fiber optic measuring system. The FOA-2000 uses lenses to guide the optical energy from the monochromator to the fiber [8]. The use of off-axis paraboloidal mirrors would require redesigning of key components of our system, such as the base plate, input / output alignment stepper motors, and beam switches.

Lenses are widely used to guide visible light in optical systems. Most lenses are made of fused silica which has an excellent transmittance in the visible and near infrared. Unfortunately fused silica absorbs most of the spectral energy when operating around 2.7 μm. Other dielectric materials such as Lithium Fluoride, Zinc Sulfide, and Barium Fluoride can be used when operating in the mid - infrared region. These lens materials all have approximately 90% transmittance when operating between 0.6 μm and 4 μm as shown in Figures 21, 22, and 23.

All spherical dielectric lenses experience spherical and chromatic aberrations. These aberrations cause the image at the focal distance to be blurred. Spherical aberration arises from the spherical shape of the lens. The aberration causes the parallel rays that are farther from the optical axis to refract more strongly than the paraxial rays (rays that are close to the optical axis). This refraction results in a shorter focal length for the rays operating near the optical axis. Chromatic aberration is caused by the refractive index of the lens material changing as a function of optical wavelength. The refractive index is related to the focal length of a thin lens by the equation,

$$(1/f) = [n(\lambda)-1] \bullet (1/R_1 - 1/R_2), \qquad (4.3.1)$$

where $n(\lambda)$ is the refractive index of the material, R_1 is the radius of curvature of the front surface of the lens, R_2 is the radius of curvature of the back surface of the lens, and f is the focal length of the lens. When the index of the material changes as a function of wavelength, equation 4.3.1 describes the change in focal length.

Multi-element lenses like microscope objectives are widely available in fused silica but lenses made of other dielectric materials are more difficult to obtain. Infrared Optics Inc. in Farmingdale, New York, will produce multi-element infrared lenses made of Barium Fluoride, Lithium Fluoride and Zinc Sulfide designed to be mounted on the existing FOA-2000 lens mounts. Our multi-element lenses will correct for almost all spherical aberrations when operating between 0.6 μm and 4 μm, and chromatic aberration will be partially corrected when operating between 1 μm and 4 μm. According to Infrared Optics Inc., a spot size of 35 μm can be achieved at the focal point their multi-element lenses.

Our multi-element infrared lenses will experience approximately 15% more loss than the off-axis paraboloidal mirrors. The two element lens will still allow 81% of the incident power to be transmitted . The easy substitution of the infrared lenses for the fused silica lenses on the FOA-2000 makes up for this drawback. Our system, using infrared lenses, can implement all existing FOA-2000 components except for the source, monochromator, and detector. This option will require minimal modification of an existing FOA-2000 fiber optic analyzer. A specification of multi - element lens design by Infrared Optics Inc. is presented in Table 4.1.

4.4 Optical Detector

The optical photodetector used on our system must effectively operate in the wavelength region between 0.6 μm and 4 μm. Unfortunately, a single detector does not possess the sufficient detectivity to cover this broad spectral range. Two detectors will be used on the IR fiber measurement system. A -20° C cooled Germanium (Ge) detector can operate between 0.6 μm and 1.8 μm, and a 77 K cooled Indium Antiminide (InSb) detector will be used for the spectral region between 1.9 μm and 4 μm [27]. Some basic detector terminology will be presented, and the two selected detectors will be discussed in detail.

There are two main classes of photodetectors; photoemissive devices that emit photoelectrons into a vacuum or gas and solid state devices, which transport excited charges within the solid by holes or electrons. Photoemissive devices were not considered for our system because they have poor responsitivity beyond 1.2 μm. The solid state photodetectors have a variety of applications and are fabricated from a wide range of materials such as Si, InSb, Ge, PbSe, InAs [27].

The spectral performance of a given detector is usually described by the responsivity (R) or specific detectivity (D*). Responsivity is defined as

$$R = (V_s) / (H \bullet A_d), \tag{4.4.1}$$

where V_s is the output RMS voltage, H is the irradiance on the detector in watts / cm^2, and A_d is the active area of the detector in cm^2. Responsivity can not compare sensors of different areas or different electronic bandwidths so specific detectivity is used to compare different detectors. Specific detectivity is defined as

$$D^* = (A^{1/2} \bullet B^{1/2}) / (NEP), \tag{4.4.2}$$

where A is the area of the detector , B represents the electrical bandwidth, and NEP is the noise equivalent power. NEP is defined as the radiant flux incident on the detector required to yield a signal to noise power ratio of 1. The specific detectivity of Ge is shown in Figure 24, and Figure 25 illustrates the specific detectivity of mid-infrared solid state detectors [27].

The InSb and Ge detectors for the IR fiber measurement system are cooled to increase their specific detectivity. Thermal excitation, which obscures the signal, is more prominent when operating in the infrared. The Ge detector will be electrically cooled to -20° C and the InSb detector will be cooled to 77 K with a dewer filled with liquid nitrogen. The 0.25 mm diameter Ge detector is manufactured by EG & G Judson, and is currently used on the FOA-2000. The cool filtered 0.5 mm diameter InSb detector is manufactured by Infrared Associates. The cool filter reduces the photon noise by restricting stray radiation from collecting on the detector. The specific detectivity for the InSb detector used in our measurement system is shown in Figure 26 [28].

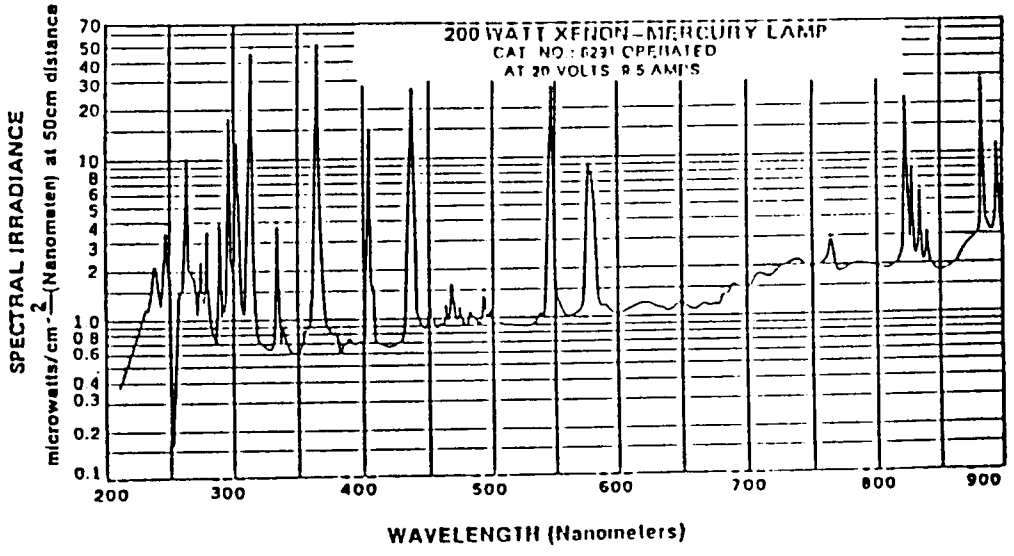

Figure 11. Spectral Irradiance of an Arc Lamp [12]

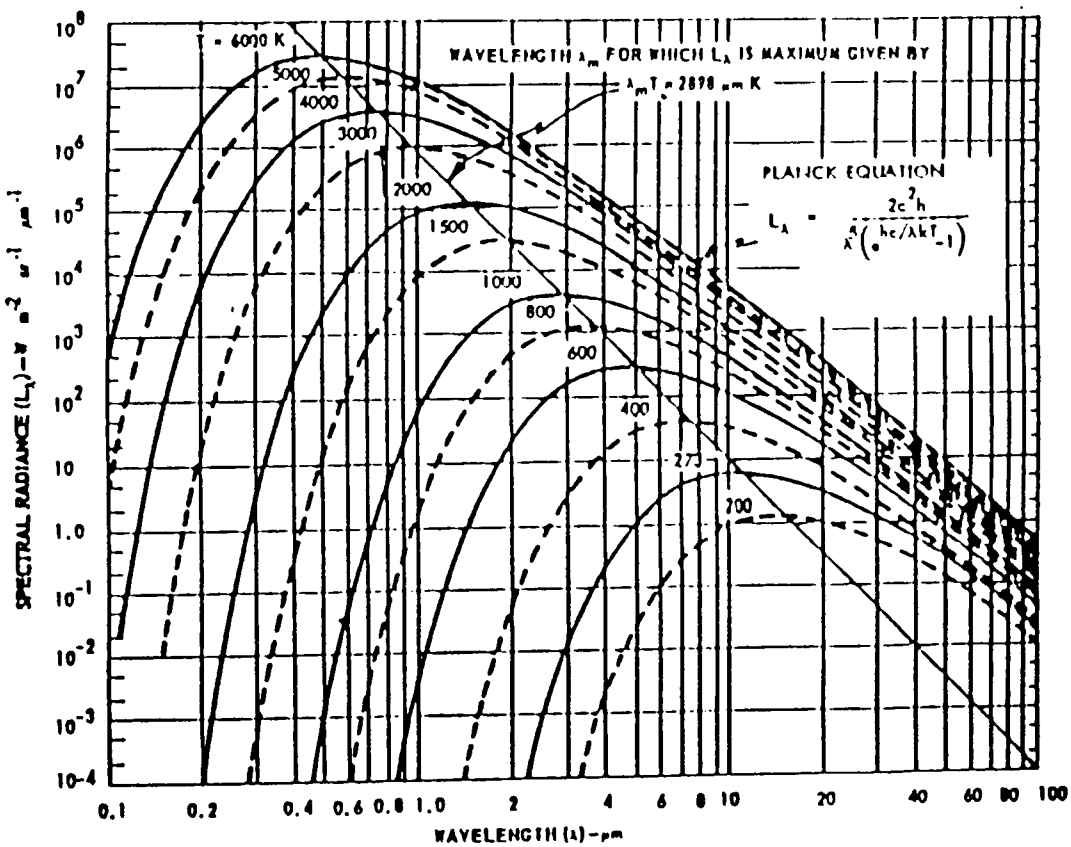

Figure 12. Spectral Irradiance of Blackbodies [12]

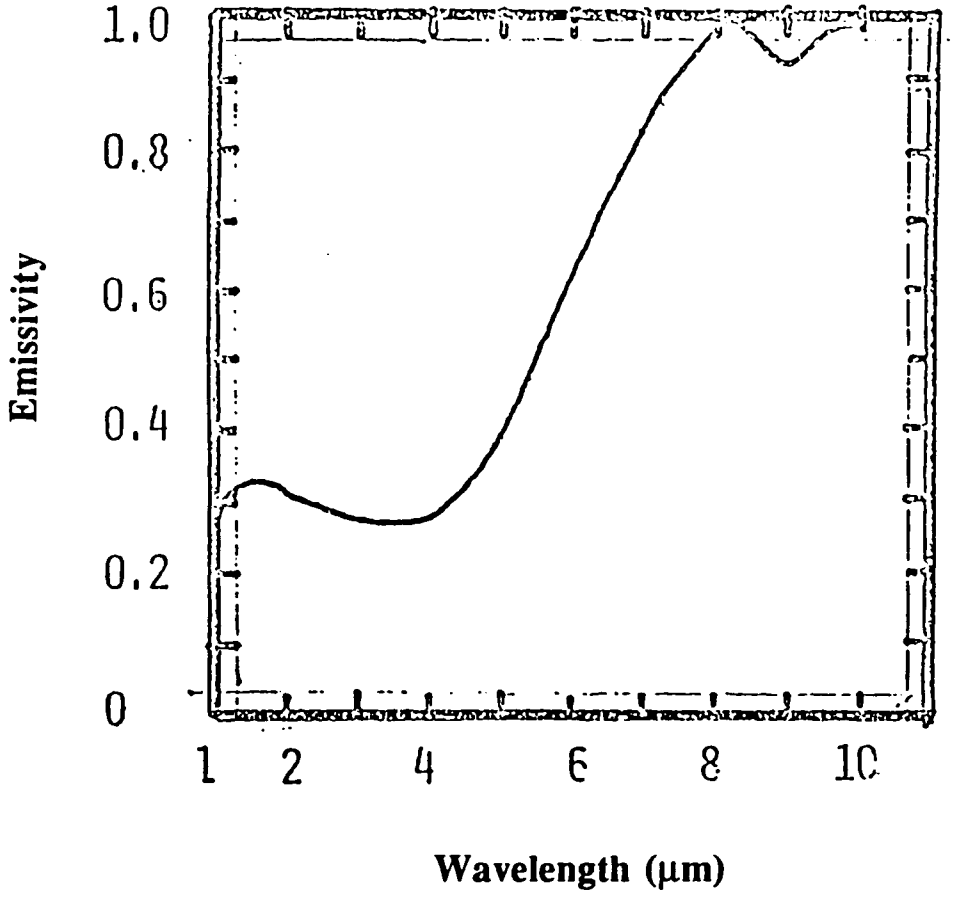

Figure 13. Emissivity of Nernst Glower at 2000°k [17]

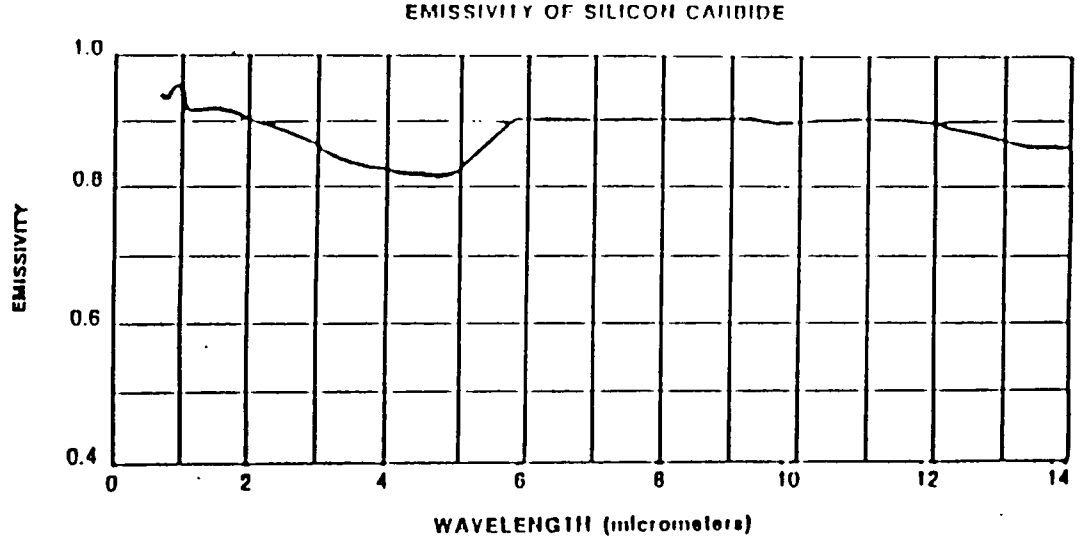

Figure 14. Emissivity of Silicon Carbide [12]

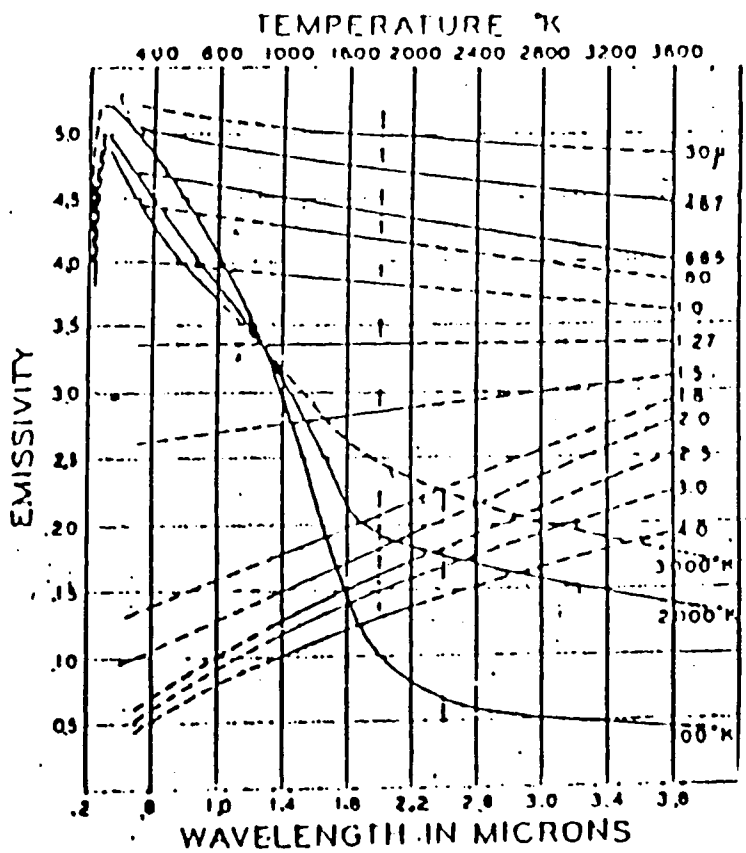

Figure 15. Emissivity of Tungsten [16]

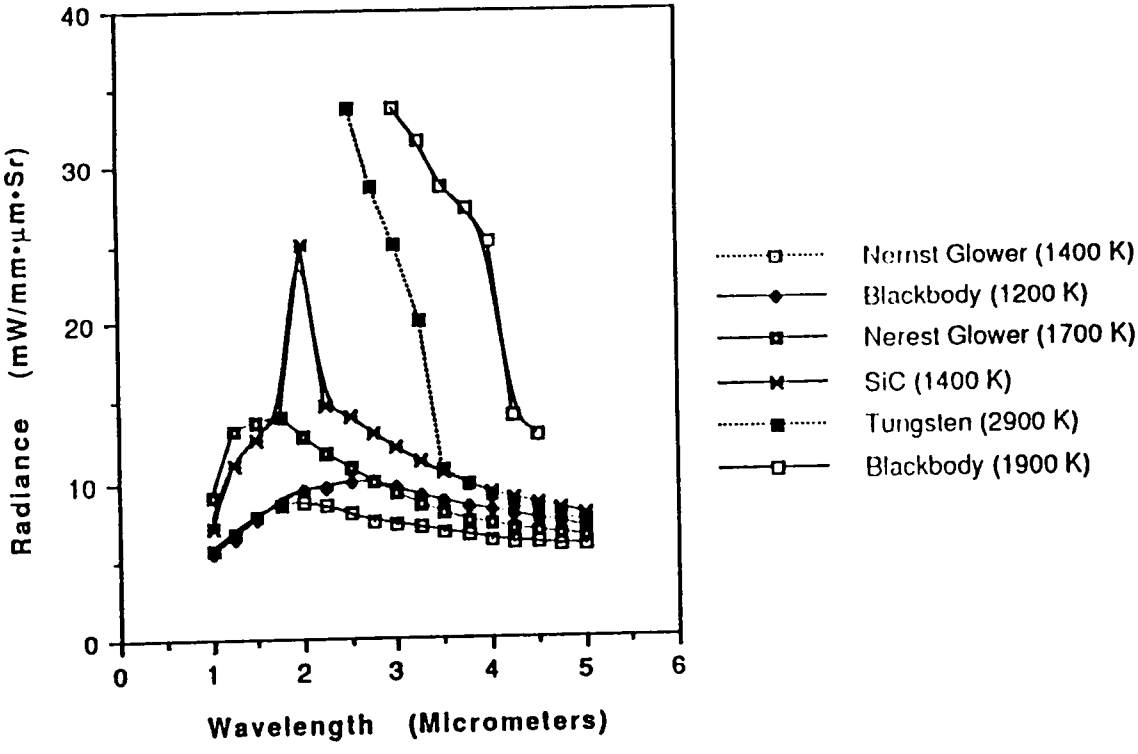

Figure 16. Radiance Test Performed by K. Harding [17]

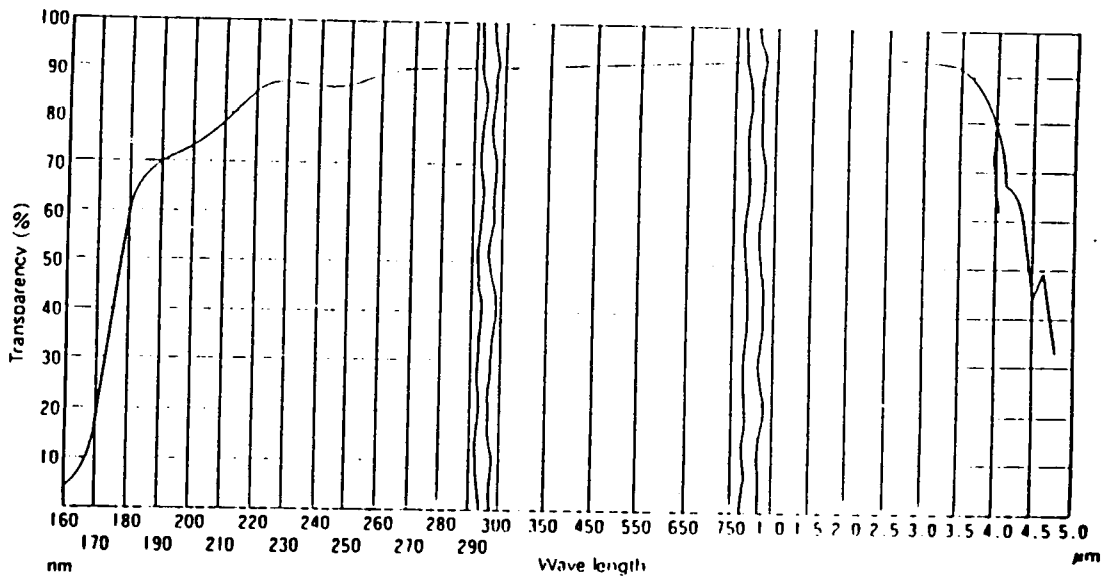

Figure 17. Transmittance of Ushio Quartz Envelope [20]

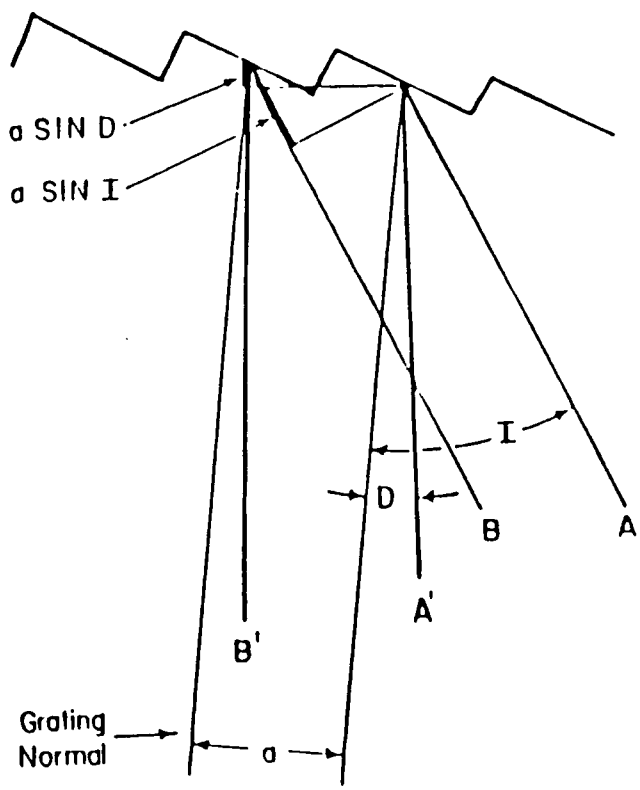

Figure 18. Grooved Grating [12]

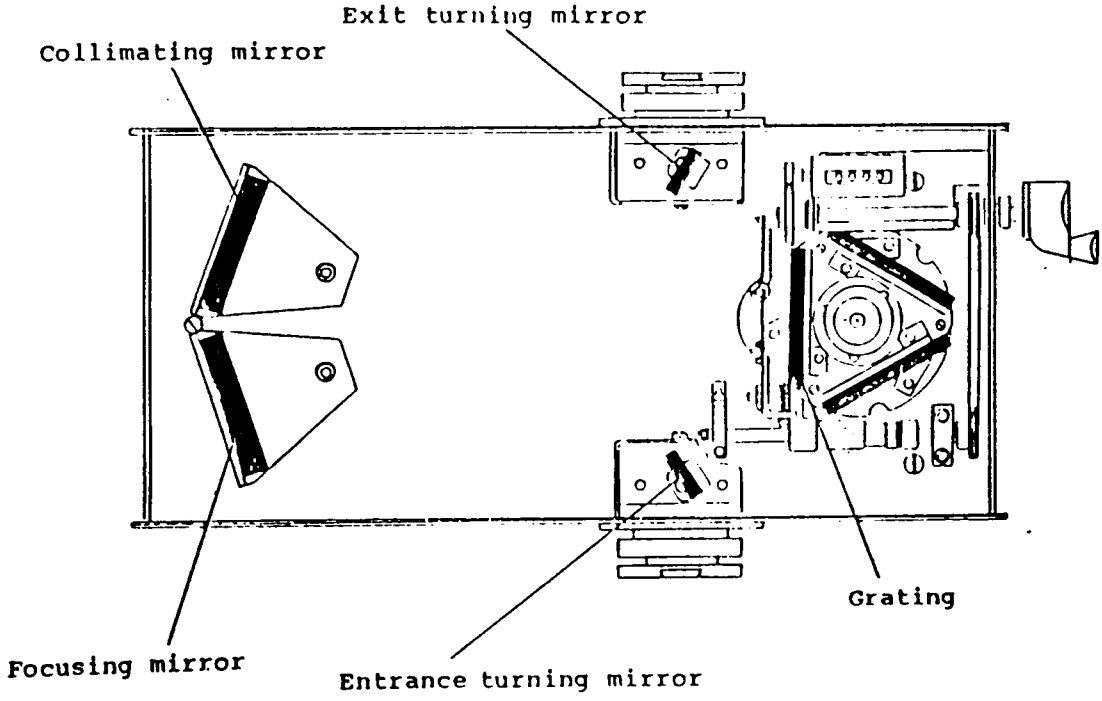

Figure 19. Jarall Ash Monospec 27 Monochromator [21]

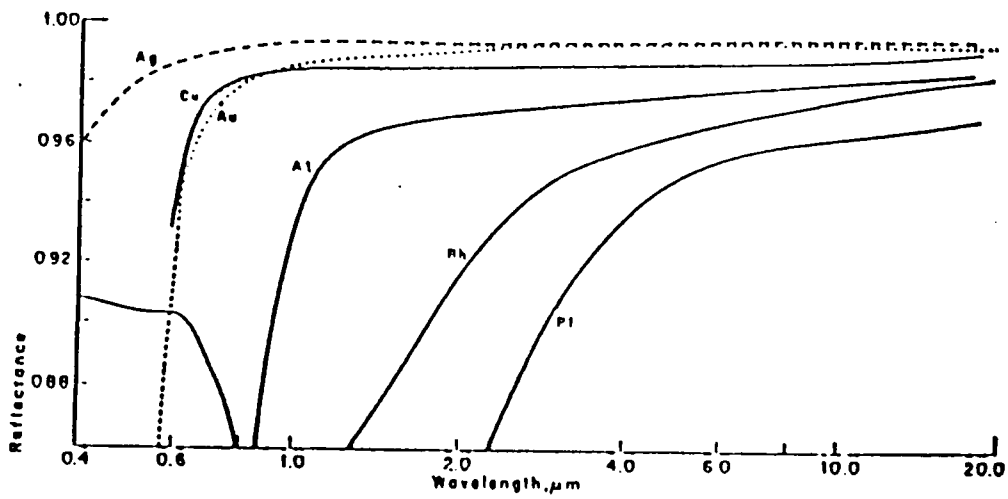

Figure 20. Reflectance of Metals [23]

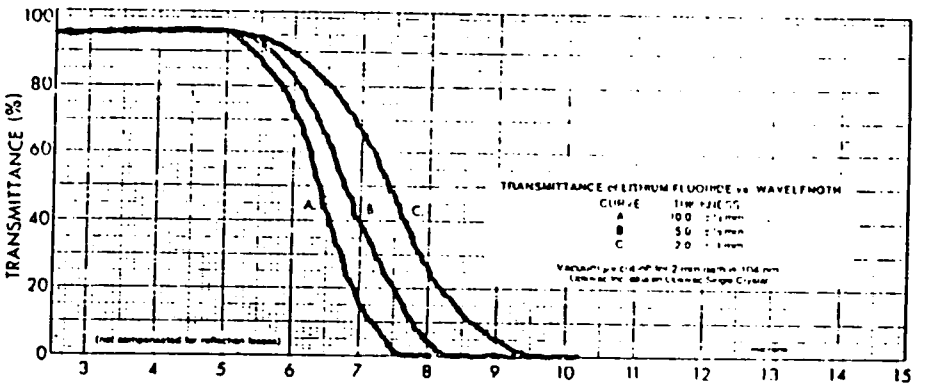

Figure 21. Transmittance of Lithium Fluoride [23]

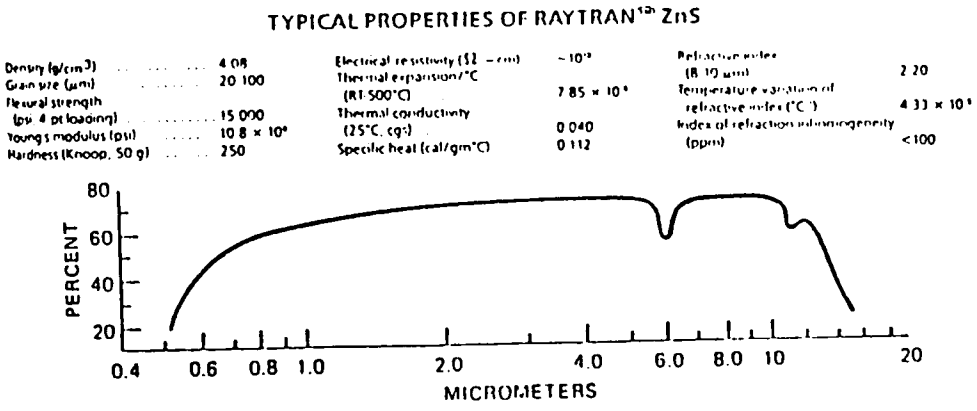

Figure 22. Transmittance of Zinc Sulfide [23]

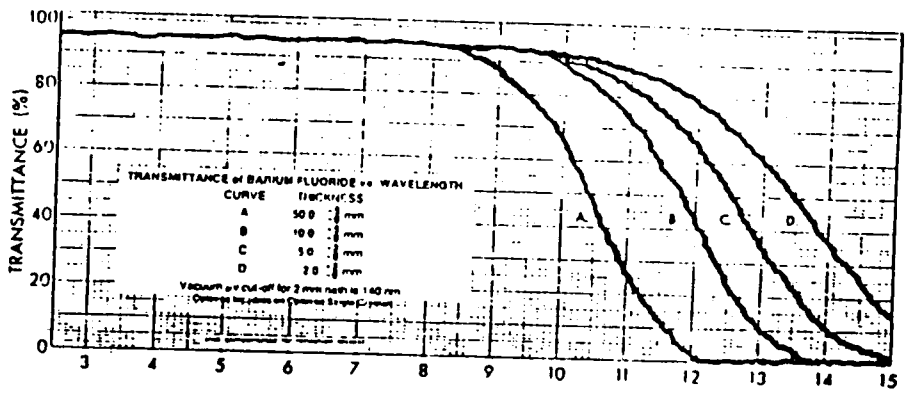

Figure 23. Transmittance of Barium Fluoride [23]

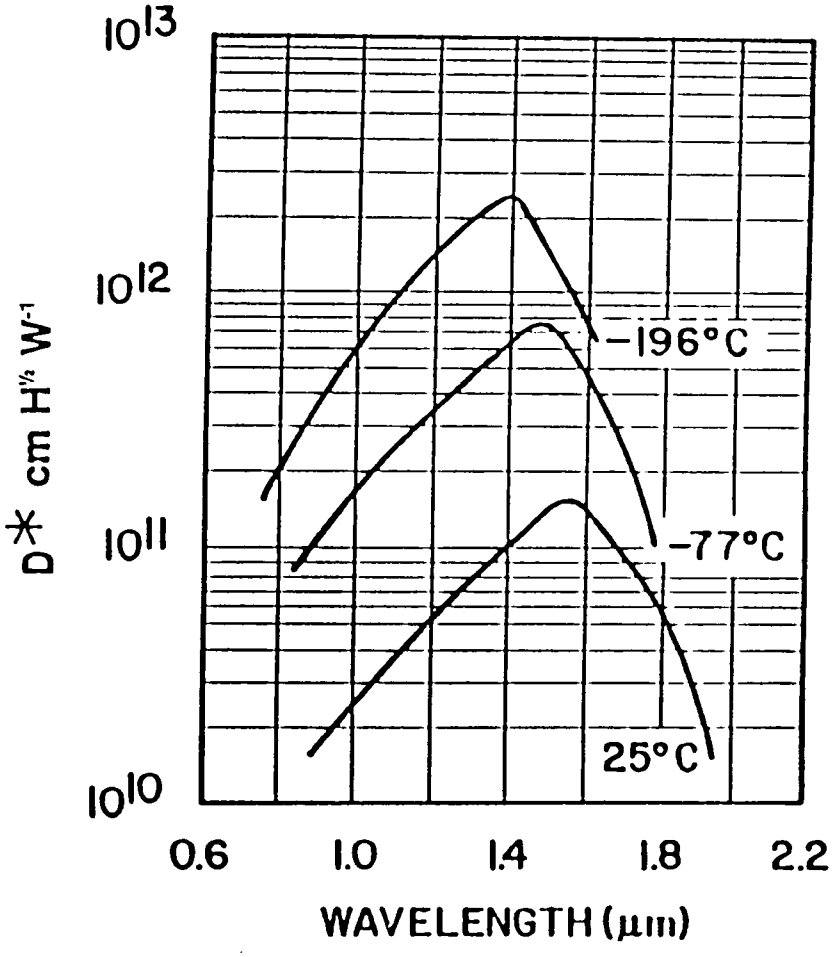

Figure 24. Specific Detectivity of Ge [12]

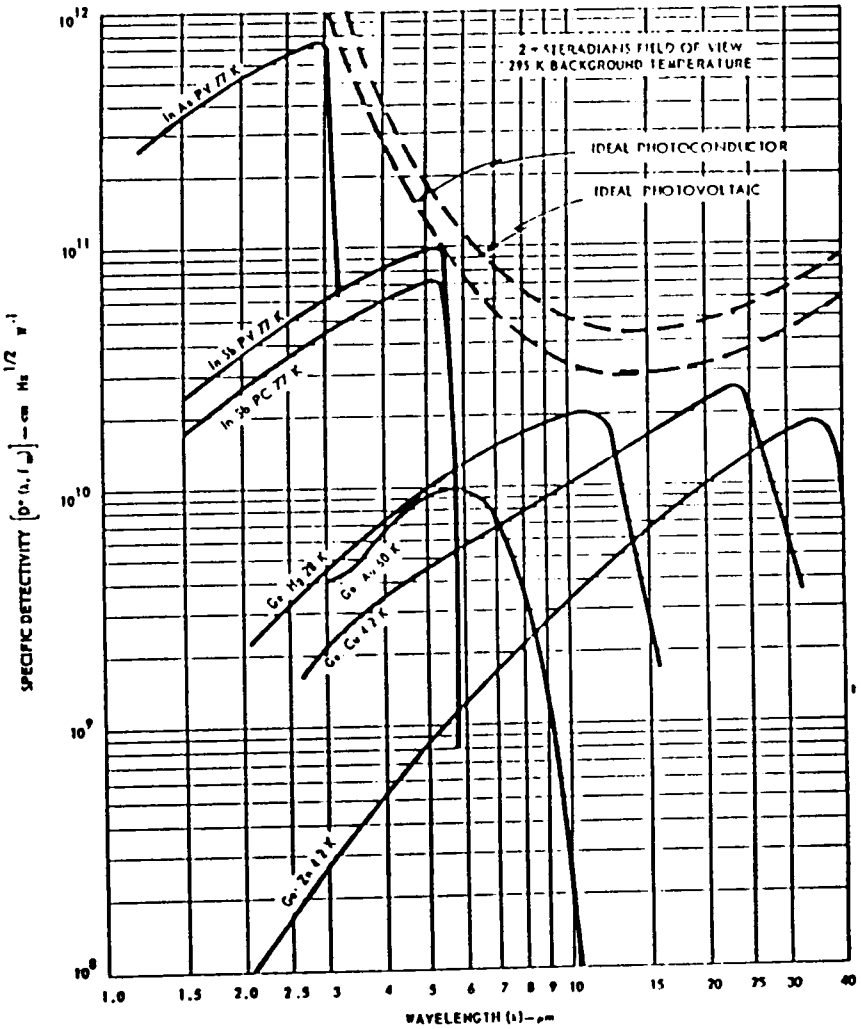

Figure 25. Specific Detectivity of IR Solid State Detectors [27]

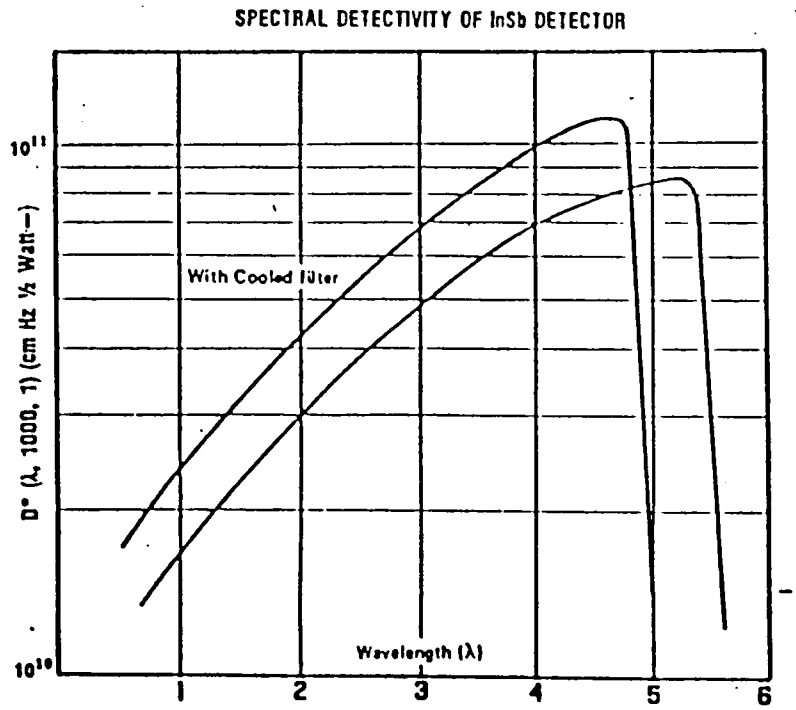

Figure 26. Specific Detectivity of InSb Detector Produced by Infrared Asso. [28]

	LENS #1	LENS #2	LENS #3	LENS #4
FOCAL LENGTH	100mm	9mm	30mm	10mm
NUMERICAL APERETURE	0.1	0.25	0.13	0.5
NUMBER OF ELEMENTS	2	2	2	2
MATERALS USED	BaF LiF	BaF LiF	BaF LiF	ZnS

Table 4.1. Infrared Lens Specification [34]

5.0 Measurement System

The infrared fiber optic characterization system that measures spectral attenuation, differential modal attenuation, and far field radiation pattern is shown in Figure 28. All components on the FOA-2000 are used in our system except for the source, monochromator, lenses, filters, and detectors. After the initial alignment, all measurement routines are computer controlled. The computer obtains and calculates the measured data for the operator. The results are presented to the operator by a graph or table. The alignment procedure will be described in this chapter. The techniques and optical components involved in each measurement will also be presented.

5.1 System Alignment

Accurate, repeatable fiber measurement can only be performed when the optical components and the input / output fiber ends are placed at a fixed reference position [14]. The optical component alignment and the pre-measurement alignment are performed to

obtain these positions. Optical component alignment is performed only once, while pre-measurement alignment is required before each measurement set. The optical component alignment is accomplished first and will align all the optics on the measurement bench at 2.5 μm, the average operating wavelength. The pre-measurement alignment uses the adjustable input / output microscope objectives to initially place the fiber ends at the 2.5 μm focal points of these lenses. The importance of the alignment routines and a discussion of each alignment procedure will be presented in this section [8].

5.1.1 Optical Component Alignment

The optical component alignment is the most important adjustment on the fiber optic characterizer. The overall alignment of the measurement system is determined by this initial adjustment. This alignment procedure must be performed accurately to assure the reliability of the pre-measurement alignment. If both alignments are properly done, accurate repeatable measurements can be obtained. All devices on the measurement system will initially be aligned at 2.5 μm. The optical component alignment used by Photon Kinetics Corporation will be presented in this section [8].

All components on the measurement system, except for the beam switches, must be removed before optical component alignment can begin. Two short silica fibers with 50 μm core diameters are placed on the input and output fiber chucks. Two 633 nm lasers are then used to launch light into the ends of both fibers. The input / output lenses will focus

and center the fiber outputs on the alignment target placed at the edge of the optical bench. The target location, predetermined by Photon Kinetics Corporation, assures the correct placement of the fiber output in relation to the input / output fiber lenses. Using the aligned input /output fibers, the mirrors on the beam switches are individually aligned. The fiber output images are centered on the alignment target which are placed in predetermined slots near each beam switch. The 275 mm lens, CID array camera, and two specular mirrors are placed and aligned on the optical bench using the output fiber and alignment target. The 850 nm LED is is also placed on the system [8].

The focal length of all the lenses in the system increase as wavelength increases. This increase is due to chromatic aberrations. The change in focal length verses wavelength of the 100 mm lens and the 9 mm lens is shown in Figure 28a, and 28b. This lens information was obtained from the lens manufacturers, Infrared Optic Inc. Figure 28b determines the change in focal length of the input / output fiber lenses between the wavelengths 0.633 μm and 4 μm. The change in focal length information is used to move the output fiber lens to the 2.5 μm focal length. The input fiber should be removed from the bench and the other end of the output fiber placed into the input fiber chuck. The 850 nm LED is then used to launch power into the fiber. The image of the output fiber is focused on the camera by moving the 275 mm lens. This procedure establishes the 2.5 μm focal point for the output fiber lens. The LED, monochromator, launch spot control, and the output alignment target are also aligned by focusing their images on the camera by adjusting the 100 mm lenses [8].

5.1.2 Pre-Measurement Alignment

The pre-measurement alignment procedure places the input / output fiber ends at a consistent location before each set of measurements. This fixed location provides maximum power launch into the input fiber ends. This location is determined in the component alignment procedure. The pre-measurement alignment procedure ensures consistent launch conditions for all fibers measured on the system. The alignment guarantees that the image of the launch spot will be located in the center of the fiber. It also aligns the fiber ends to the 2.5 μm focal length of the input / output lenses. The output fiber end will be consistently aligned for maximum power collection by the Ge and InSb detectors. The pre-measurement alignment can be manually performed by viewing the fiber ends on the CID array camera. The CID array camera is connected to a TV screen which has a predetermined outline of the fiber location on the screen. When the fiber is imaged and focused on the outline, the fiber ends are aligned on the system. A software-controlled automated alignment procedure can be used in conjunction with the manual alignment to place the fiber ends at the reference point even more accurately. The automatic alignment involves the use of the LED, detector, launch spot control, output alignment target, and input / output lenses. The LED is used to launch the 850 nm light into the fiber. The components involved in the pre-measurement alignment will be presented in this section [8].

The components involved in the pre-measurement alignment are highlighted in Figure 29.

The power from the LED is guided to beam switch 3, where a half mirror is engaged. The half mirror allows the reflection of the input and output fiber ends to reach beam switch 4. Beam switch 4 allows the CID array camera to collect the fiber end image information. The input / output fiber lenses are adjusted until a focused image of the fiber ends is seen on a viewing monitor, which is connected to the camera. This helps the operator check the fiber end quality and also places the fiber lenses approximately at the reference point. The launch spot control is engaged, and the computer moves the input fiber lens in the x,y,and z directions until maximum power is incident on the detector. The launch spot control restricts the spot size on the input fiber end. This procedure aligns the center of the fiber on to the launch spot control because maximum power is usually concentrated in the center of the fiber. The output alignment target is then used to align the output fiber using the same procedure as the input fiber alignment. When using the output alignment target the fiber reference point yields the maximum power reading. The x, y, z input / output fiber lens positions are initialized to zero on the FOA-2000 command console. The reference position places the fiber ends at the focal point of the fiber lenses at 2.5 μm. The focal length of the fiber lenses changes due to chromatic aberrations. An x, y, z position table for the input fiber lens position is established in the FOA-2000 software, which corrects for chromatic aberrations [8].

The monochromator wavelength must also be initialized to its null order before any measurement is performed. The null order wavelength position allows all wavelengths to pass undiffracted through the monochromator slit [21]. This position must be recorded on the FOA-2000 control console. This initial recording allows the motorized monochromator to accurately obtain other wavelengths. An optical switch places the monochrometer wavelength near the null order, and then operator manually fine tunes the wavelength selector to that position by viewing it on the video display. The three gratings are pre-

aligned to have the same null order wavelength position [8].

5.2 Spectral Attenuation

The spectral attenuation measurement determines scattering and absorptive loses in a fiber as a function of wavelength. This measurement can help determine the causes of extrinsic and intrinsic loss, because certain loss mechanisms occur at particular operating wavelengths [9]. Our system will measure spectral attenuation of step index fibers for the wavelength region between 0.6 μm and 4 μm with overfilled launch conditions. The fiber core will be overfilled and the numerical aperture (NA) of the source will exceed the fiber NA. A high index fluid will be applied to the cladding periphery to eliminate the cladding modes. The overfilled launch conditions are not the most accurate way to measure low loss fibers, but because of the high extrinsic losses of fluorozirconate fibers the error due to overfill is negligible [14]. When the extrinsic losses of ZrF_4 fibers are reduced, a steady state modal power distribution must be achieved to obtain accurate spectral attenuation. A mode mixing technique to reach steady state modal power distribution is presented. The cutback technique is introduced in this section as a means of obtaining the attenuation value. A description of the system alignment and the components involved in the measurement routine is also addressed.

5.2.1 Cutback Technique

The cutback technique is the most widely used method to measure total spectral transmission loss of fiber cables. A test fiber of length L is excited with a monochromator at an initial wavelength, and an output power $P_{\lambda 1}(L)$ is recorded by the computer. The monochrometer is then set at the next wavelength and the power $P_{\lambda 2}(L)$ is recorded. This process continues until all desired wavelengths from the monochromator are scanned. The fiber is then cut to about a meter in length without changing the source and launch conditions. The monochrometer is again set to the initial wavelength , and an output power $P_{\lambda 1}(L=1m)$ is recorded. $P_{\lambda 1}(L=1m)$ is approximately the power launched into the test fiber of length L at the particular wavelength λ_1. This approximation is valid because the loss in one meter of fiber is negligible. The cutback power is measured for each λ_n. The loss in the fiber in dB/km for a particular wavelength is calculated by the computer using equation,

$$\text{Loss}\lambda_n(\text{dB/m}) = 10\text{Log}_{10}[P_{\lambda n}(L=1m)/P_{\lambda n}(L)]. \qquad (5.2.1)$$

The cutback method can result in substantial error if care is not taken to keep the initial launch conditions constant . Cutback should be performed at the output end of the fiber to keep the fiber launch conditions constant. A precise cleaver should be used to ensure constant flat cleaves of the input and output fiber ends. When fiber ends are not consistently flat, accurate repeatable measurements can not be obtained [14].

5.2.2 Steady State Modal Distribution

The power flow in a single mode fiber or for a particular mode in a multimode fiber can be described by the formula,

$$P(z) = P(0) \cdot e^{-2\alpha z}, \qquad (5.2.2)$$

where P(0) is the power launched into the input fiber end. P(z) is the power in the fiber at a distance z from the input fiber end and 2α is the power loss coefficient. However, particular modes in a multimode fiber have different power loss coefficients, thus the total power flow cannot always be described by equation 5.2.2. However, there are some conditions for the power flow in a multimode fiber that can be described by equation 5.2.2. These conditions can occur when mode coupling or mode mixing is strong enough to cause the distribution of power over the various modes to reach a steady state condition. The launch conditions do not affect the power distribution of the modes once a steady condition is met [14].

The fiber steady state condition must occur to accurately and repeatedly measure fiber attenuation, especially for fibers with low loss. A mode scrambler may be used to reach the steady state condition. A short portion of the test fiber is forced into sinusoidal bends,

which causes mode mixing to occur. The cladding modes can be removed by dipping the fiber cladding in index matching fluid [14].

5.2.3 Spectral Attenuation Measurement Routine

The system is ready to perform spectral attenuation measurements after the alignment procedure is completed. The optical path and the components involved in this measurement are shown in Figure 30. The operator selects the desired wavelength interval on the computer. An HP computer then relays that information to the FOA -2000 command console, which sets the monochromator wavelength to the beginning of the interval. At the end of the chosen wavelength interval, the computer will automatically stop the wavelength scanning by the monochromator. The light from the monochromator passes through the cutoff filter, which blocks the higher order spectra output by the monochromator. The image of the output monochromator slit is enlarged by 10/3 at the chopper, which modulates the signal at 165 Hz. The beam switches maintain the light in the correct direction. The large 100 mm lenses act as anti-vignetting lenses which help maintain the light in the correct optical path. The power from the monochromator is launched into the input end of the test fiber. The power from the output end of the fiber is either collected by the Ge detector or the InSb detector. The Ge detector is used for the wavelength between 0.6 μm and 1.79 μm, and the InSb detector operates between 1.8 μm and 4 μm. These

detector operating wavelengths are used because the specific detectivity of InSb is higher than Ge between 1.8 μm and 4 μm. The switching between the detectors are automatically performed by the HP computer. The detectors are connected to a lock-in amplifier, which picks up the modulated 165 Hz signal. The voltage information from the lock-in is recorded into the HP computer for this particular wavelength. The monochromator then scans the next wavelength and the light follows the same previous optical path. The voltage output of the lock-in amp is once again recorded [8].

After all the desired wavelengths are scanned by the monochrometer and the power is collected by the detector, the monochrometer wavelength is reset to the original starting wavelength. The test fiber is also cut to about one meter without disturbing the input fiber end. The entire power collecting sequence is then repeated using the shorter fiber. The spectral attenuation of the fiber is calculated by the computer using the cutback equation 5.2.1 which was described earlier [8].

5.3 Differential Modal Attenuation

Differential modal attenuation measures the optical fiber loss as a function of the different mode orders. Mode dependent loss measurements can describe the different loss mechanisms in fibers. In low-loss waveguides, intrinsic material loss mechanisms such as Rayleigh scattering, ultraviolet absorption, and infrared absorption are obtained. The causes of other intrinsic waveguide losses, such as leaky modes and finite cladding

thickness, are obtained by differential modal attenuation. In high loss waveguides, extrinsic losses such as impurities, diameter variations, or other geometric irregularities can be observed with mode dependent attenuation measurements [29]. The material information obtained from these measurements can obviously be used to reduce waveguide attenuation.

Our measurement system will selectively excite different mode orders of step-index fibers by using spatial filters and spot size restrictors. In the next section a proof of this technique is presented using geometric optics.

5.3.1 Differential Modal Attenuation Scheme

The geometrical optics or ray method is an effective means of analyzing multimode optical fibers. The ray method is only useful when the wavelength is much smaller than the dimensions of the waveguide. Weakly guiding multimode fibers satisfy this condition so ray analysis is applicable. A ray represents the direction of energy flow of an electromagnetic wave with a constant phase plane perpendicular to the ray path. If rays are used in analyzing optical fibers, then localized electromagnetic plane waves of the form

$$\vec{E} = \vec{e}(r)e^{-jk_0\phi(r)} \tag{5.3.1}$$

$$\vec{H} = \vec{h}(r)e^{-jk_0\phi(r)} \tag{5.3.2}$$

are solutions in the optical fiber waveguide [14]. The scalar function $\phi(r)$ describes the phase at position r, while k_0 is the free space wave number. The eikonal equation,

$$(\nabla\phi)^2 = n^2(r), \tag{5.3.3}$$

is obtained when equations 5.3.1 and 5.3.2 are substituted into Maxwell's equations. $\nabla\phi$ represents lines normal to the phase front surface, and n(r) is the refractive index of the medium. $\hat{s}$ is a unit vector along the ray path and can be expressed as,

$$\hat{s} = \frac{d\vec{r}}{ds}. \tag{5.3.4}$$

The unit vector $\hat{s}$ can also be written as,

$$\hat{s} = \frac{\nabla\phi}{|\nabla\phi|}, \tag{5.3.5}$$

where $|\nabla\phi|$ is the magnitude of $\nabla\phi$. When the eikonal equation is substituted into equation 5.3.5, $\hat{s}$ takes on the form,

$$\hat{s} = \frac{\nabla\phi}{n(r)} = \frac{d\vec{r}}{ds}. \tag{5.3.6}$$

The ray equation,

$$\frac{d}{ds}\left[n(r)\frac{d\vec{r}}{ds}\right] = \nabla n(r), \tag{5.3.7}$$

can be obtained if both sides of equation 5.3.6 are differentiated with respect to s [14]. For

step-index fiber $\nabla n(r)$ equals to 0 because the refractive index of the core and cladding are constants. The ray equation for step-index fibers can be expressed as,

$$\frac{d}{ds}\left[n(r)\frac{d\vec{r}}{ds}\right] = 0. \tag{5.3.8}$$

The cylindrical coordinate system is used for the cylindrical fiber geometry. The position vector in this coordinate system is expressed as,

$$\vec{r} = x\hat{a}_x + z\hat{a}_z. \tag{5.3.9}$$

The substitution of 5.3.9 into 5.3.8 results in two differential equations,

$$\frac{d}{ds}\left[n\frac{dx}{ds}\right] = 0 \tag{5.3.10}$$

$$\frac{d}{ds}\left[n\frac{dz}{ds}\right] = 0. \tag{5.3.11}$$

The solutions to equation 5.3.11 can be expressed as,

$$n\frac{dz}{ds} = \bar{\beta}, \tag{5.3.12}$$

where $\bar{\beta}$ is a constant and also the normalized propagation constant,

$$\bar{\beta} = \frac{\beta}{k_0}. \tag{5.3.13}$$

With the help of Figure 31, it is easily seen that,

$$\frac{dz}{ds} = \cos\theta. \tag{5.3.14}$$

For guided rays in the core, equation 5.3.12 can be expressed as,

$$\cos\theta = \frac{\bar{\beta}}{n_1}, \tag{5.3.15}$$

where n_1 is the refractive index of the fiber core [30]. Equation 5.3.15 shows the relationship between the normalized propagation constant and the steepness of the ray hitting the core cladding interface. The normalized propagation constant decreases when θ increases for a fixed wavelength of operation. When the normalized propagation constant decreases higher order modes will propagate when the operating wavelength is fixed. The relationship between the angle of the ray entering the fiber from air and the refracted ray in the fiber can be expressed as,

$$\sin\varepsilon = n_1 \sin\theta, \tag{5.3.16}$$

where ε is the angle of the ray entering the fiber from air, and θ the refracted ray in the fiber. Equation 5.3.15 can be reexpressed in terms of ε by using equation 5.3.16 [30]. If equation 5.3.16 is substituted into equation 5.3.15, the equation,

$$\sin\varepsilon = \sqrt{n_1^2 - \bar{\beta}}, \tag{5.3.17}$$

is obtained. Equation 5.3.17 relates the angle of the ray entering the fiber with the normalized propagation constant and the refractive index of the core.

The technique used to excite the different mode order for the differential modal attenuation

measurement is shown in Figure 32. The spot size of the light on the fiber is approximately 35 μm or approximately 1/3 the core diameter of a 100 μm core fiber. The center of the spatial filter is placed at the left focal point of the fiber input lens and the center of the fiber core is at the right focal point of the input fiber lens. The placement of the spatial filter is critical because parallel rays to the right of the lens will correspond to a particular point on the left focal plane.

The sketch of the annular spatial filter apertures used to excite mid and high order modes is shown in Figure 33. The low order modes are excited with small circular apertures. The dimensions of the apertures were obtained from the equation,

$$\theta = \tan^{-1}\left[\frac{f}{2h}\right], \tag{5.3.18}$$

where f is the focal length of the input fiber lens, h is the full clear aperture, and θ is the maximum half angle of the meridional ray entering the input fiber [26].

This technique by no means will excite exact mode orders due to aberrations in the lenses and diffraction effects from the aperture. The scheme will excite a set of mode groups.

5.3.2 Differential Modal Attenuation Measurement Routine

There is a separate software routine to perform differential modal attenuation but the routine is similar to that used for spectral attenuation measurement. The differential modal

attenuation measurement routine is identical to the spectral attenuation measurement procedure except for the use of the launch spot size restrictor and the spatial filters. The operator selects and manually places the spatial filters onto the measurement system before each set of measurements. The launch spot controller is automatically set in place by the computer. The cutback technique is also employed for differential modal attenuation measurements.

5.4 Far Field Radiation Pattern

The infrared fiber optic characterizer will perform far field radiation pattern measurements at 1.55 μm and 2.55 μm for step index ZrF_4 fibers. This measurement technique can reveal relevant fiber parameters for the fiber designer such as numerical aperture (NA). The purpose of the far field measurement is briefly discussed next, followed by a description of the spatial scan far field measurement technique. An optical layout and the instruments involved in the measurement is also presented.

5.4.1 Purpose of Far Field Scan

The far field scan determines the effective numerical aperture of the fiber, which may be different from the calculated NA value if differential modal attenuation or mode coupling is present. The calculated NA or real NA for step index fiber is defined as,

$$NA = n\mathrm{Sin}\theta_m = \frac{n_1^2 - n_2^2}{2n_1} \qquad (5.4.1)$$

where θ_m is the largest angle of a meridional ray which can be guided in the fiber. The refractive index that surrounds the fiber is n while n_1 and n_2 represent the core and cladding refractive indices [31].

The far field scan can describe transmission properties of multimode fibers, such as impulse response and coupling efficiency. Other fiber parameters, such as differential modal attenuation and mode coupling can be deduced when the effective NA value is different from the calculated value [37]. Experiments have shown that when significant differential modal attenuation is present the effective NA value is smaller than the calculated value. When mode coupling is present the effective NA value is greater than the real value [32].

5.4.2 Spatial Scan Technique

The angular scan and spatial scan measurement techniques are the only Electronic Industries Association (EIA) approved schemes to measure output far field for multimode fibers [33]. The angular scan method involves the scanning the output of the fiber in an arc, with a detector to obtain the far field. The spatial scan technique, as shown in Figure 34, uses two lenses and a translating pinhole to obtain the output far field. Lens 1 is known as the transform lens and images the far field, while lens 2 collects the intensity information and images it onto the detector [33]. The center of the fiber output is placed in the right object focal point of lens 1, while the far field scanner is located in the left image focal plane of lens 1. This set up enables all parallel ray from the fiber to be uniquely imaged on the left image plane where the angular intensity pattern is obtained [26].

The position of the linear scanner is related to the angle at which the ray exits the fiber by the equation

$$y = f \cdot \sin \theta, \qquad (5.4.2)$$

where y is the distance from the central axis in the spatial plane, f is the focal length of lens 1, and θ is the angle of the ray measured from the optical axis. Equation 5.4.2 is valid because the design of well corrected microscope objectives employs this equation. The

collected irradiance [E(y)] from the linear far field scanner must be converted to an angular intensity distribution [I(θ)]. E(y) and I(θ) are related by the formula

$$I(\theta) = E(y) \cdot \cos\theta \text{ [33].} \qquad (5.4.3)$$

The Photon Kinetics FOA-2000 uses the spatial scan technique. Additional lenses are used to image the far field aperture to the left image plane of output fiber lens, because there is not enough space to directly place the scanner there. An example graph of far field scan performed by the FOA-2000 is shown in Figure 35. The sine (angle) corresponding to the 5% intensity is the numerical aperture [8].

The far field measurement routine on the FOA-2000 uses a powerful 850 nm LED source to launch light into the fiber. The system must perform a far field radiation scan at 1.55 μm and 2.55 μm and the monochromator is used. The monochromator outputs less power than the LED, and there is a signal to noise problem when using the monochromator and pinhole on the infrared fiber characterizer as explained in Chapter 6. The pinhole aperture can be increased in size from that used on the FOA-2000 because we are operating at a longer wavelength than the 850 nm used on the FOA-2000.

The knife edge technique is used on the infrared fiber characterizer to determine the fiber numerical aperture because the pinhole aperture does not allow enough power to reach the detector, as determined in Chapter 6. This procedure is used to find the mode field diameter of single mode fibers [38]. The top edge of the far field scanner is used instead of the pinhole in the knife edge technique. This technique gives the integration of the angular intensity distribution out of the fiber as shown in Figure 36 a. If the data in Figure 36 a is differentiated, the numerical aperture of the fiber can be obtained but some far field

radiation pattern information is lost due to the differentiation. Fiber numerical aperture measurements using the knife edge technique are not mentioned in the EIA far field measurement specifications, but the method does give an approximate fiber numerical aperture.

A far field scan, using the knife edge technique and the pinhole technique, was performed at 850 nm with the FOA-2000. A 1 km, 50 μm core, mulitmode fiber was used as the test sample for both measurements. The far field pattern using the pinhole technique is shown in Figure 36 c. A numerical aperture of 0.233 was obtained with the pinhole method. An integrated far field scan using the knife edge technique is shown in Figure 36 a. Piecewise numerical differentiation was performed on the curve of Figure 36 a and the result is shown in Figure 36 b. Three measurements of far field scan were performed using the knife edge technique, and the numerical aperture values of 0.237, 0.238, and 0.238 were obtained. The far field scan using the knife edge technique does not present an accurate far field radiation pattern, but does provide a repeatable approximate numerical aperture value for multimode fibers.

5.4.3 Far Field Measurement System

The components involved in the far field radiation measurement routine are highlighted in Figure 37. The broad band quartz tungsten lamp illuminates the input slit of the monochromator. The monochromator selects either 1.55 μm or 2.55 μm. The cutoff

filters only allow the desired wavelength to pass while blocking out the higher order spectra. Lens 2 focuses the light onto the chopper, which modulates the signal at 165 Hz. The beam switches change the direction of light to the appropriate optical component. The adjustable input fiber lens focuses the reduced image of the monochrometer slit onto the input fiber end. The image of the slit is reduced by 3/10 at the input 9 mm lens' image focal plane. The fiber output end is placed at the output 9 mm lens' object plane. The output rays from the fiber are analyzed with the movable far field pinhole scanner and the InSb detector is positioned to accept the output power. A lock-in amplifier is connected to the optical detector to retrieve the 165 Hz signal. An HP computer controls the movement of the far field scanner while collecting and storing the voltage readout from the lock-in amplifier. The measurement ends with the HP computer's plot of the far field radiation pattern [8].

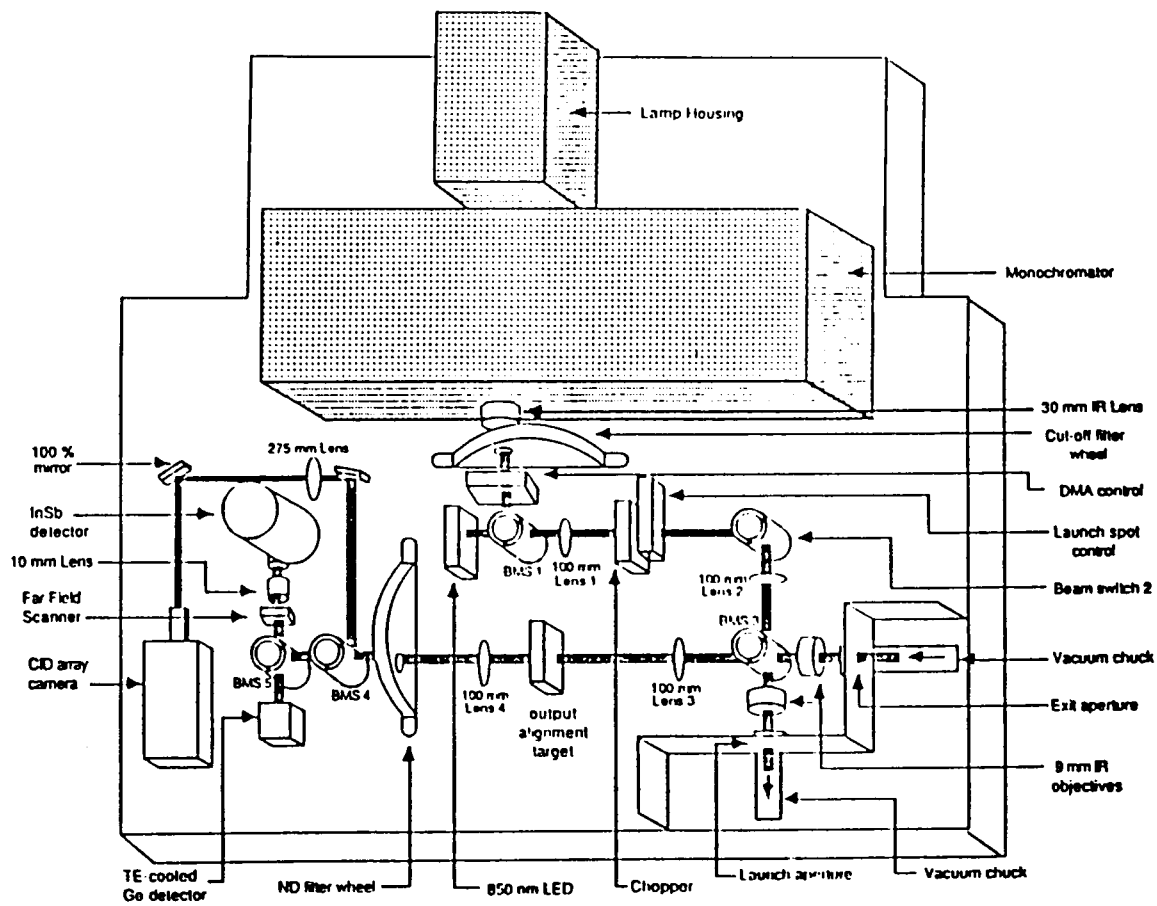

Figure 27. System Diagram of the IR Fiber Optic Characterizer

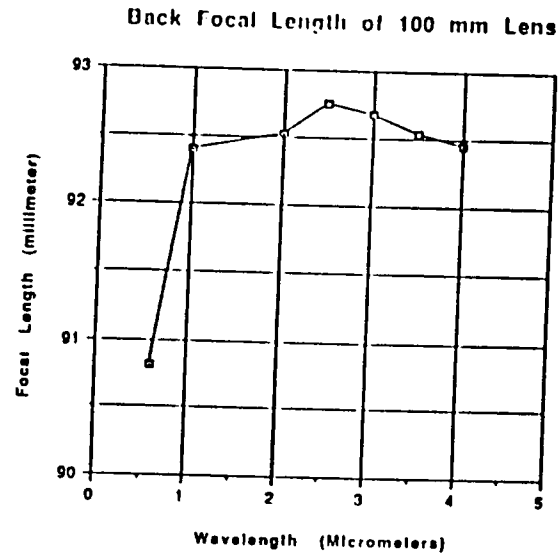

(a)

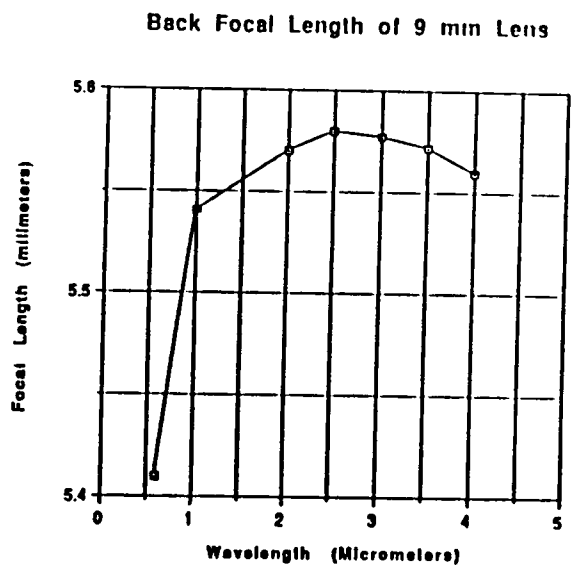

(b)

Figure 28. Back Focal Length of (a) 100 mm Lens [34] (b) 9 mm Lens [34]

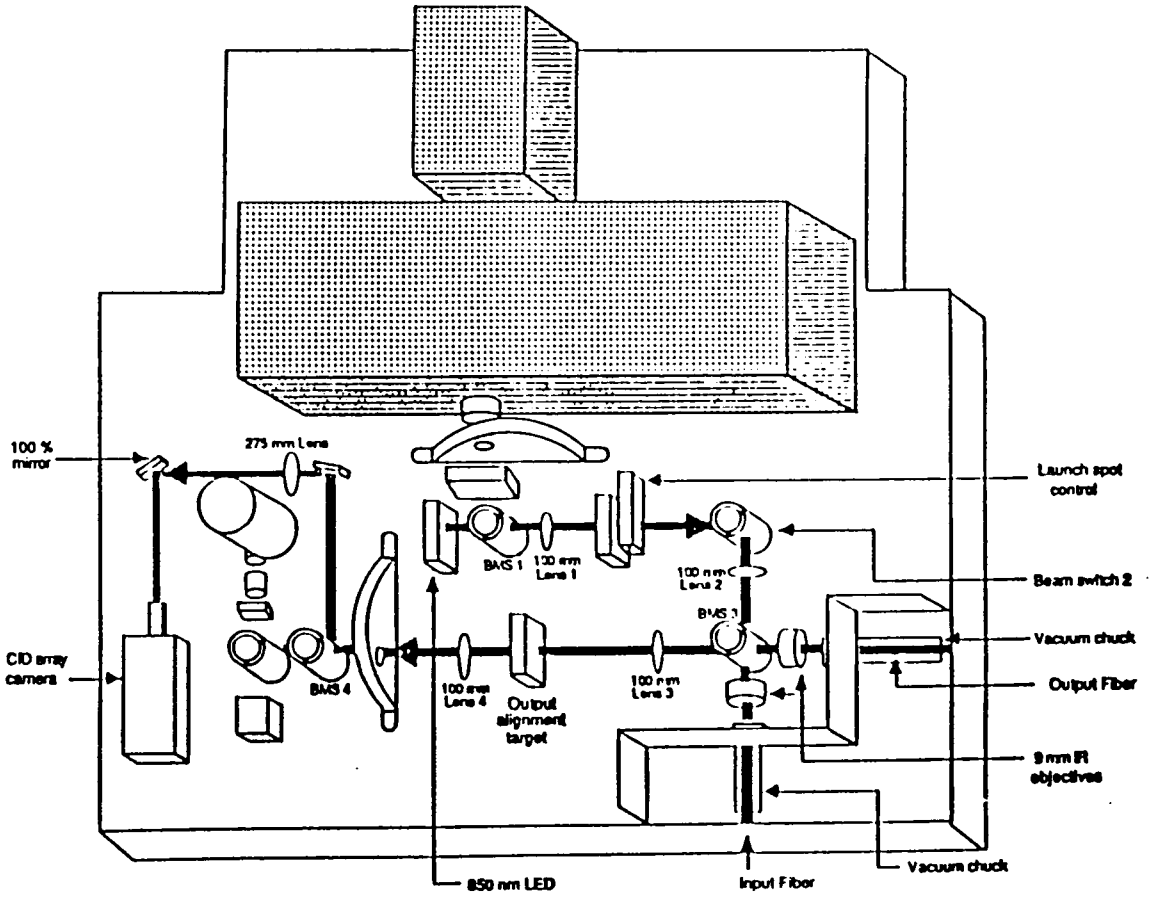

Figure 29. Components Involved in the Input/Output Fiber Alignment

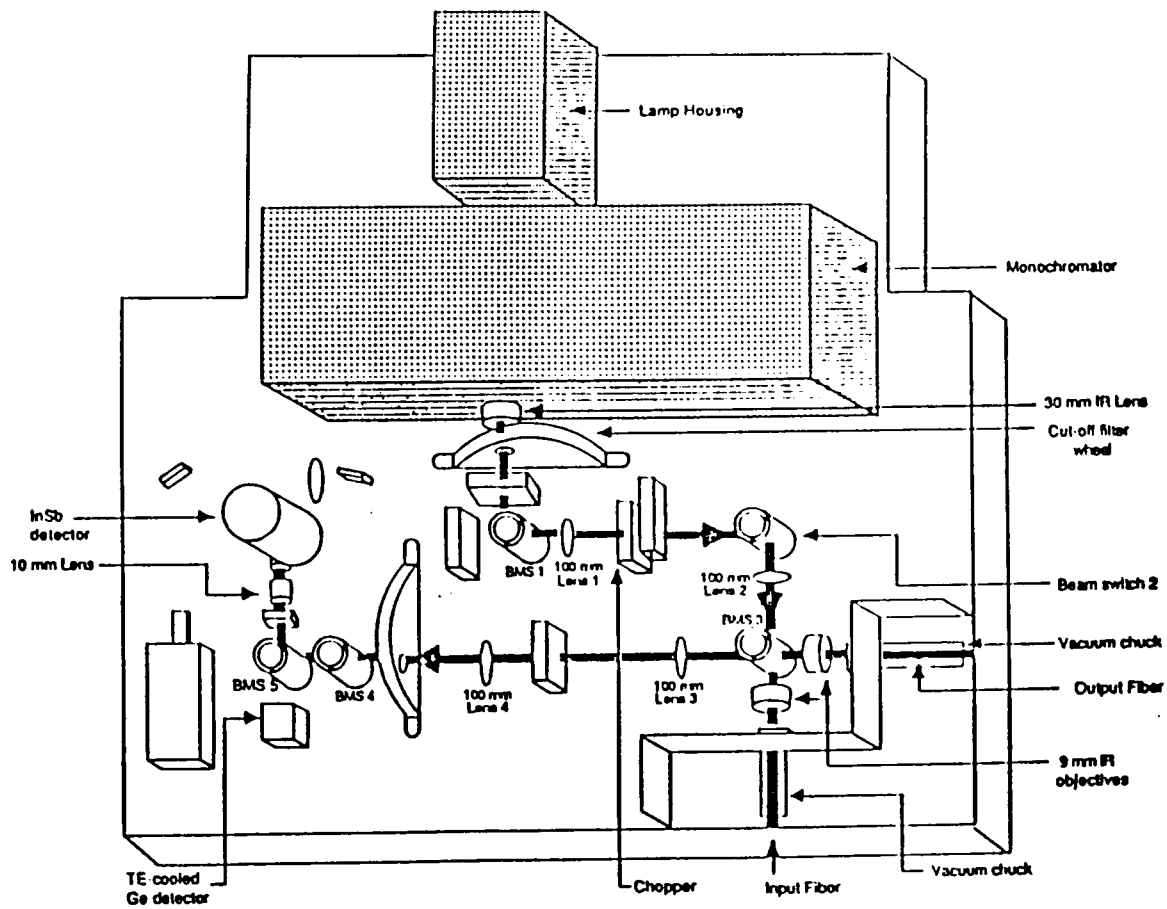

Figure 30. Optical Components Involved in Spectral Attenuation

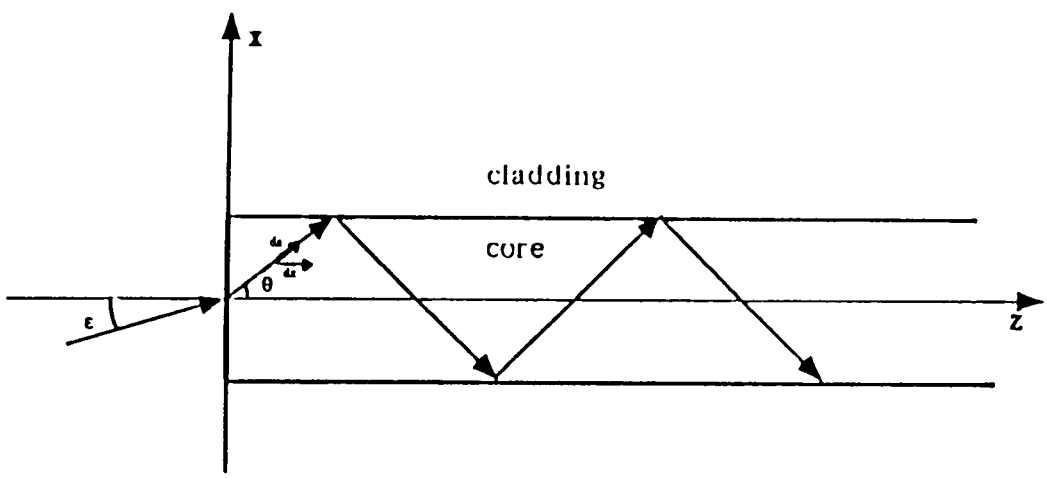

Figure 31. Projection of a Ray onto the ϕ = Constant Plane

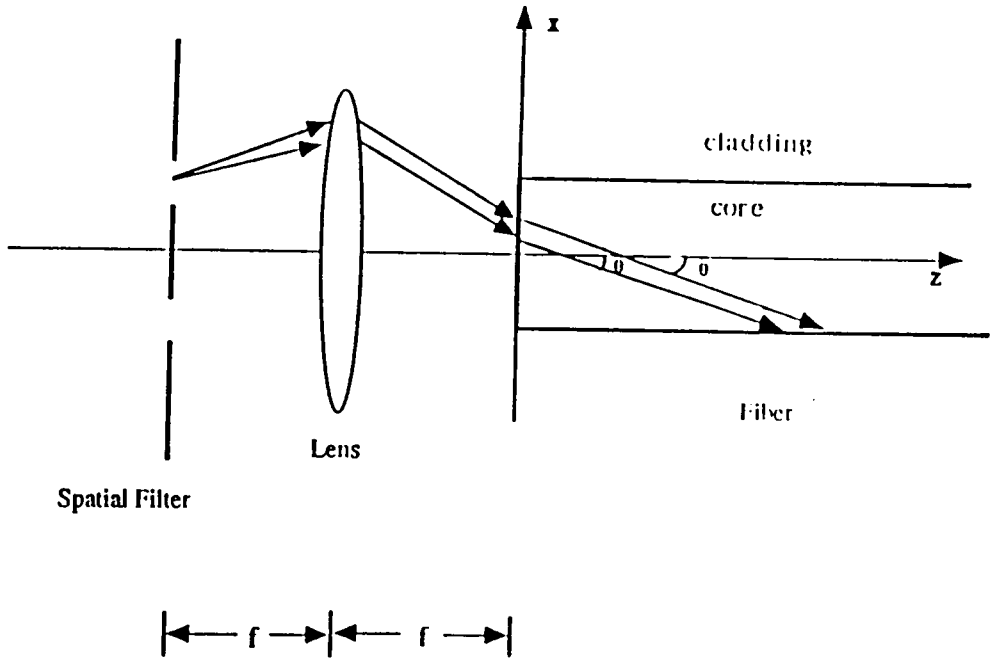

Figure 32. Scheme to Excite Different Mode Orders

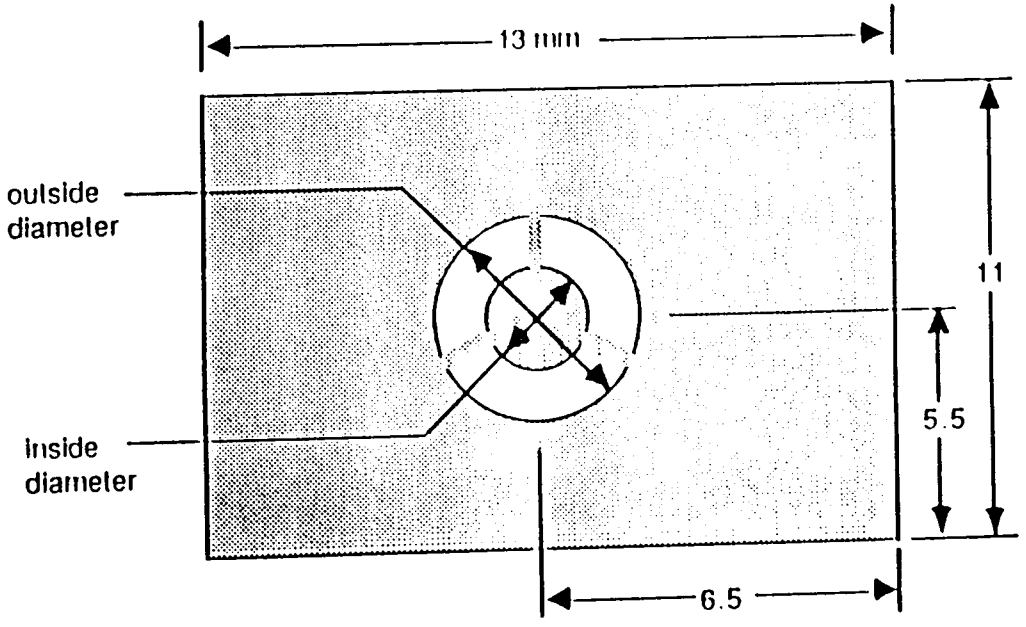

Figure 33. Annular Aperture

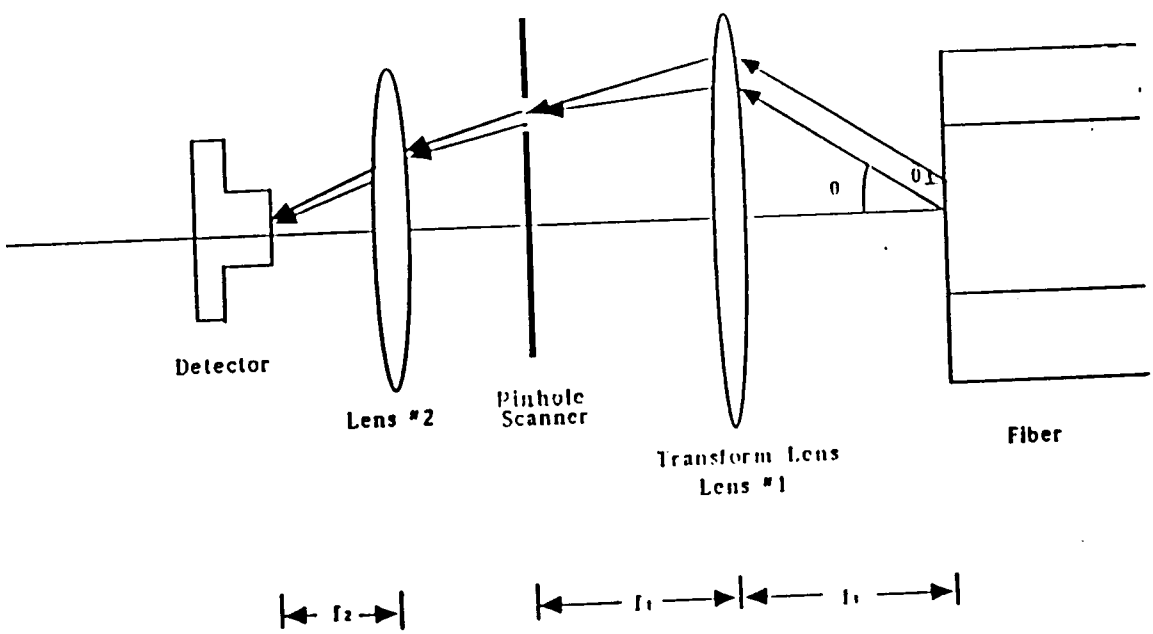

Figure 34. Linear Far Field Scanner

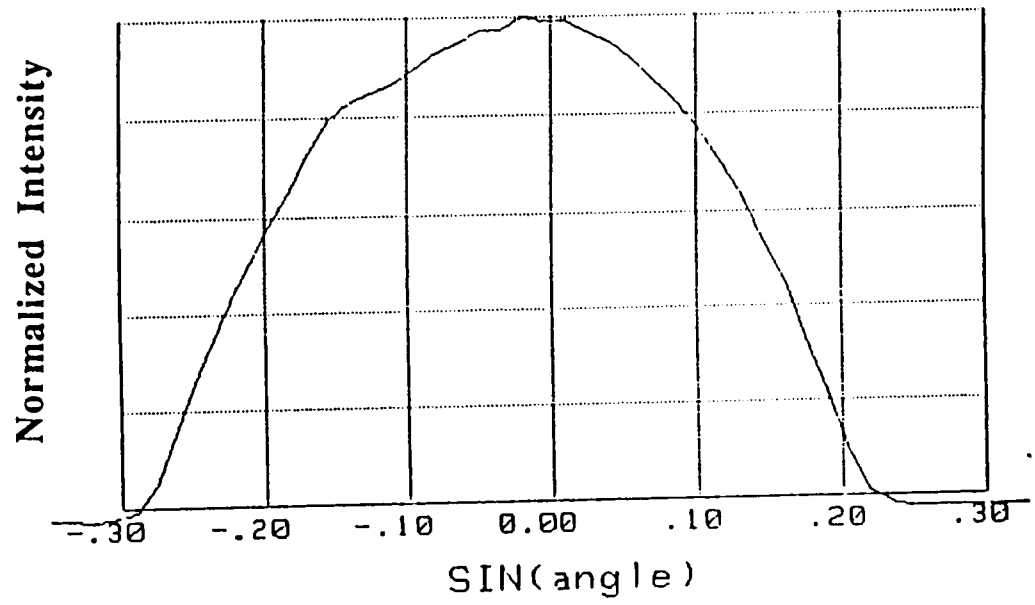

Figure 35. Typical Far Field Scan Result on the FOA-2000

(a)

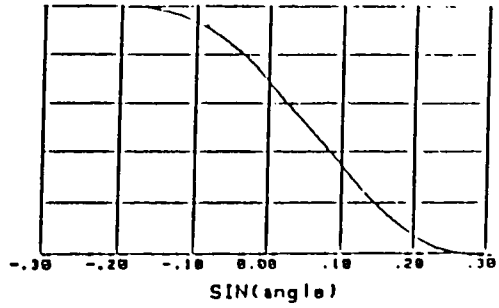

(b)

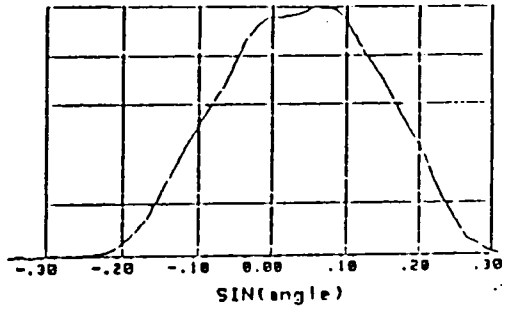

Numerical Aperture = .238

(c)

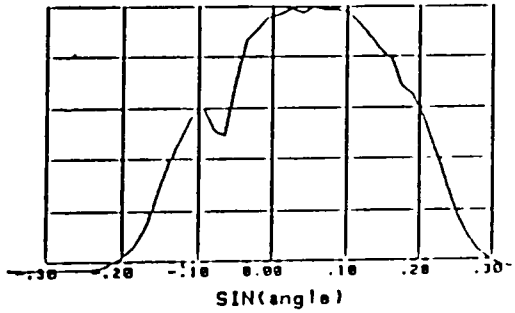

Numerical Aperture = .233

Figure 36. Far Field Scan Performed on the FOA-2000 by (a) Knife Edge Technique (b) Knife Edge Technique and Differentiation (c) Pinhole Scan

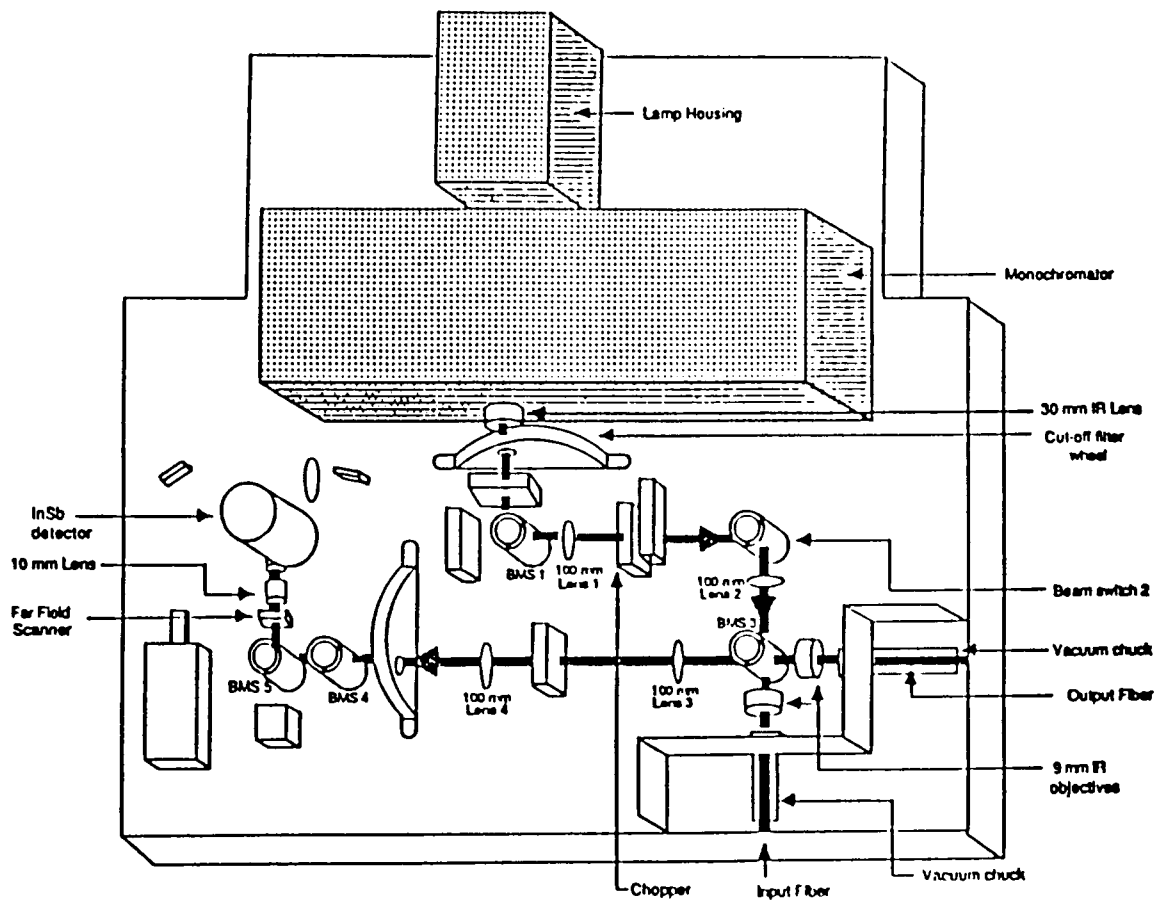

Figure 37. Optical Components Involved in Far Field Scan

6.0 Testing the System

After the measurement system was constructed and aligned, the optical component alignment procedure was used to align the machine. The system was then tested to determine how much power was launched into the fiber and the amount of power that was received by the detector. The system wavelength scan error was also tested by using the spectral attenuation measurement routine without cutback. The accuracy and repeatability of the measurement routines was also tested. The testing of the constructed system will be addressed in this chapter.

6.1 Power Launch into Fiber and System Accuracy

There are two system parameters that can help the operator determine the maximum fiber loss the measurement system can handle. These parameters are the signal received by the

detector out of a short length of fiber and the average noise recorded by the lock-in amplifier. High losses in the fiber cause smaller portions of the launched power to be registered on the lock-in amplifier. If the fiber output signal approaches the noise signal of the detector accurate measurements cannot be obtained.

The system wavelength scan error test can help determine the wavelength error caused by the fluctuation of the source, stray light onto the optical detector, and monochromator scanning errors. The monochromator scanning error occurs when the monochromator wavelength has shifted during cutback [8]. The shift in wavelength is caused by the inherent errors in the movement of the mechanical parts on the monochromator. The wavelength scan error test does not include the errors due to inconsistent launch conditions and fiber end quality. The procedure and the results of the approximate signal launched into the test fiber will be presented in this section, and the system wavelength scan error test is also discussed in this section.

The following test describes the routine used to measure signals received by the detector when using a short length of fiber. A one meter, 52 μm core diameter, silica fiber was used. The ends of the fiber were aligned using the CID array camera. Grating 1 in the monochromator was scanned between 0.8 μm and 1.8 μm. The Ge detector was used to collect the power emitted by the fiber output. A lock-in amplifier was connected to the Ge detector, and the voltage information was recorded by the computer. Figure 38 illustrates the signal received by the lock-in amplifier when using monochromator grating 1 and the Ge detector. The figure also compares the outputs obtained using the 1 mm monochromator and 0.5 mm monochromator slits. The bandpass for the 1 mm slit using grating 1 is approximately 6 nm and the bandpass for the 0.5 mm slit is approximately 3

nm for the same grating. As can be expected, the 1 mm slit provides approximately twice the transmitted power as the 0.5 mm slit [21].

The wavelengths between 1.8 μm and 4 μm are covered by monochrometer gratings 2 and 3. A one mm monochrometer slit was also used to restrict the spectral bandpass. A one meter, 100 μm core diameter fluorozirconate fiber and an InSb detector were used in this higher wavelength range. The voltage readings on the lock-in amplifier when using gratings 2 and 3 are shown in Figure 39. The signal recorded on the lock-in amplifier when using the InSb detector and grating 2 and 3 is approximately 21 dB lower than when using the Ge detector in the shorter wavelength range. Part of the signal difference is attributed to the detectors. The specific detectivity of InSb over its operating range is approximately eight times or 9 dB less than that of Ge when operating in its wavelength range [12, 27]. The quartz-tungsten lamp also emits approximately two times less power or 3 dB less at 3.4 μm than at 1 μm as shown in Figure 15. The emissivity of a 3000 K tungsten at 1 μm and 3.4 μm is approximately 0.4 and 0.2, respectively.

The reduced power recorded at the longer wavelengths may also be attributed to the inherent properties of the monochrometer gratings, optical filters, lenses, and/or the quartz envelope surrounding the tungsten source. The loss in the short ZrF_4 fiber used in the test may also reduce the power reading on the lock-in amplifier. Figure 39 shows a severe power drop at 2.72 μm by both gratings 2 and 3. This drop indicates that factors other than the gratings may be attributed to the minimum power reading. This drop in power reading may be caused by the filters, the lenses, and/or the quartz envelope.

The reduced power at the longer wavelengths will not allow the accurate measurement of

fibers with high loss. If the ZrF_4 fibers possess high attenuation then shorter lengths can only be characterized for spectral attenuation, differential modal attenuation and numerical aperture. The noise signal generated by the InSb detector registers approximately 1 μV on the lock-in amplifier over the entire operating range of the detector. This noise value was obtained by covering the detector's active area from all stray light and recording the average signal fluctuation on the lock-in amplifier. The minimum power from the monochromator occurs at 2.7 μm and grating 3 was used at this wavelength. This minimum power point assumes negligible loss in the one meter ZrF_4 fiber. The power reading on the lock-in amplifier at 2.7 μm is 0.477 mV, which gives a minimum signal-to-noise ratio of 26.7 dB. The 26.7 dB signal-to-noise ratio does not account for the stray light from the monochrometer and/or room light received by the detector. Higher power results are obtained when the system operates between 0.8 μm and 1.8 μm than when operating at the longer wavelengths. When using the 1 mm monochrometer slit, lock-in output levels as high as 240 mV at 1.32 μm were recorded. Even operating at 1.8 μm, the wavelength yielding the lowest power reading for grating 1, 2.4 mV was recorded. The average noise signal registered on the lock-in amplifier for the Ge detector is 2 μv over its operating range. The minimum signal to noise ratio is approximately 30 dB at 1.8 μm.

The system wavelength scan error was tested by performing spectral attenuation on one meter of ZrF_4 fiber without performing cutback. The fiber ends are manually aligned with the CID array camera and monitor. The monochromator then scans the desired wavelength interval. At the end of the wavelength scan, the fiber is not perturbed in any way, and the monochromator scans the same previous wavelength interval. The results of the measurement compare signal fluctuation of the final launch signal and the previous launch signal at a particular wavelength. The power ratio between the initial wavelength scan and

final scan without cutback is zero for an ideal system without source output fluctuations and monochromator scan error. Unfortunately, the wavelength scan error on the IR fiber optic characterizer is severe at the longer wavelengths as shown in Figure 40. The high error may be attributed to stray light from the source and/or monochromator scan error.

6.2 Spectral Attenuation Measurement Test

The spectral attenuation between 0.8 μm and 1.8 μm was performed on a 740 m, graded index, 50 μm core diameter, multimode silica fiber. The measurement was first performed on the FOA-2000 and then on the IR fiber optic characterizer. The spectral attenuation measurement between 1.8 μm and 4 μm was not performed because ZrF_4 fibers shipped from NRL were extensively damaged, and the longest undamaged lengths were only 9 m long. The spectral attenuation between 0.8 μm and 1.55 μm was also performed on the FOA 2000. A graph that compares the spectral attenuation measurement test between the IR fiber optic characterizer and the FOA-2000 is shown in Figure 41. The fiber losses measured when using the FOA-2000 are generally higher than those obtained using the IR fiber optic characterizer. This difference in spectral attenuation may be caused by the IR measurement system not being aligned and/or the difference in the launch optics.

6.3 Far Field Scan Test

Far field measurement using the pinhole scanner was attempted at 1.55 μm and 2.55 μm with a short length of fluorozirconate fiber. The result as shown in Figure 42 is an erratic curve caused by the low signal power coupled out of the fiber end. The knife edge technique was then performed at 2.55 μm to compensate for this signal to noise problem at the detector. Light at 2.55 μm from the monochromator was used to launch power into a one meter ZrF_4 fiber. The cladding modes of the fiber were removed by applying IR absorbing paint on the exposed fiber cladding. The far field was scanned by the top edge of the far field scanner and the data was differentiated to obtain the knife edge far field. The measurement was repeated three times with the same fiber and the results are shown in Figure 43. The three obtained numerical aperture values are 0.084, 0.084, and 0.085. The measurement is repeatable, but is not accurate.

The accuracy of the knife edge technique employed on the infrared fiber optic cable characterizer was tested against that of the pinhole aperture method used on the FOA- 2000. The far field scan on the FOA-2000 was performed at 0.85 μm with the ZrF_4 fiber. The LED and the linear pinhole aperture were used to measure thefar field. The cladding modes

were removed by applying IR absorbing paint on the cladding surface. A fiber numerical aperture of 0.124 was obtained using the FOA-2000. The same ZrF_4 fiber was used for the far field measurement on the infrared fiber optic characterizer. The 0.85 μm monochrometer light was used to illuminate the input end of the fiber. The far field was scanned with the top edge of the linear pinhole aperture. The pinhole was covered. A numerical aperture of 0.091 was obtained with the knife edge technique. There is a large discrepancy in the far field results between the FOA-2000 and the infrared fiber characterizer.

The discrepancy in the far field results is not solely caused by the difference in the techniques. The FOA-2000 was modified to perform far field measurements using either the pinhole aperture or the top of the pinhole aperture. The 850 nm LED was used in both the pinhole and knife edge techniques. The numerical aperture result using the pinhole was 0.233 and the numerical aperture using the knife edge was 0.238 as shown in Figures 36b and 36c. The primary difference between the knife edge technique used on the infrared fiber optic characterizer and the pinhole aperture technique performed on the FOA-2000 is caused by the different focal lengths of the output fiber lenses in the two systems. The software converts the far field scanner position to the angle at which the ray exits the fiber by equation 5.4.2,

$$y = f\sin\theta.$$

The symbol y represents the distance from the central axis in the spatial plane, f is the focal length of the output fiber lens, and θ is the angle of the ray measure from the optical axis. The focal length of the output fiber lens on the infrared fiber characterizer is approximately

9 mm at 2.5 μm, while the focal length of the output fiber lens on the FOA-2000 is approximately 11 mm. When the incorrect focal length of 11 mm was used on the infrared fiber optic characterizer numerical aperture results of 0.084 and 0.085 were obtained.

The exact focal length of the output fiber lens at 1.55 μm and 2.55 μm on the infrared fiber optic characterizer is not known because the lenses have not been tested. The exact focal length of the output fiber lens may not be necessary if an accurate numerical aperture of a test fiber is known. The infrared fiber optic characterizer can be calibrated to the numerical aperture value of the test fiber by adjusting the focal length value of the input fiber lens in the software.

6.4 Differential Modal Attenuation Measurement Test

Differential modal attenuation (DMA) was only performed on silica fiber in the wavelength region between 0.8 μm and 1.8 μm due to the unavailability of ZrF_4 fibers. A 200 m, 50 μm core, 0.23 NA, step index fiber was used as the test sample. The chromatic aberration correction software was not used to correct for the change in focal length of the input fiber lens because of problems associated with the input/output fiber auto alignment. Auto alignment must be performed to run the chromatic aberration correction software. The spot

size restrictor was used but the 35 μm spot size on the input fiber end was not achieved over the tested wavelength range due to chromatic aberration. The result of the differential modal attenuation measurement may not be accurate because a spot size of 35 μm on the input fiber end was not achieved.

A test for DMA measurement repeatability was performed using a circular aperture that restricts the numerical aperture of the light into the fiber to 0.06. The measurement was repeated three times and the results are shown in Figures 44a and 44b. Figure 44b uses a reduced attenuation scale to more easily compare the lower attenuation values. The large attenuation value at 1.4 μm is a result of OH absorption [31].

Differential modal attenuation using two different circular apertures and two different annular apertures were also performed on the test fiber. The two circular apertures restrict the numerical aperture of the light into the fiber to 0.06 and 0.08. The 0.06 numerical aperture restrictor allows lower order modes to be excited than the 0.08 numerical aperture restrictor allows. The results of the attenuation values using the two circular apertures are shown in Figure 45. The use of the 0.06 numerical aperture restrictor resulted in a lower attenuation value than when the 0.08 numerical aperture restrictor was used. These compared results are typical for optical fibers on a spool; the higher order modes usually possess higher losses than the lower order modes due to microbends on the spool. The annular filters restricted the NA of the light into the fiber over the range of $0.14<NA<0.21$ and $0.11<NA<0.17$. The results of the attenuation values of these filters are also shown in Figure 45. The annular aperture which restricts the numerical aperture of the light entering the fiber over the range of $0.14<NA<0.21$ had higher attenuation values then the other annular filter. Spectral attenuation measurement was performed without the use of the

spatial filter and the results are plotted in Figure 45. The spectral attenuation measurement had the second highest loss as shown in Figure 45. Only the circular aperture with the maximum NA= 0.08 had higher loses. It is difficult to determine the accuracy of the differential modal attenuation measurement because the extrinsic loss mechanisms in the test fiber are not totally known. More tests need to be performed to determine if the spatial filters can be used to excite selective mode orders.

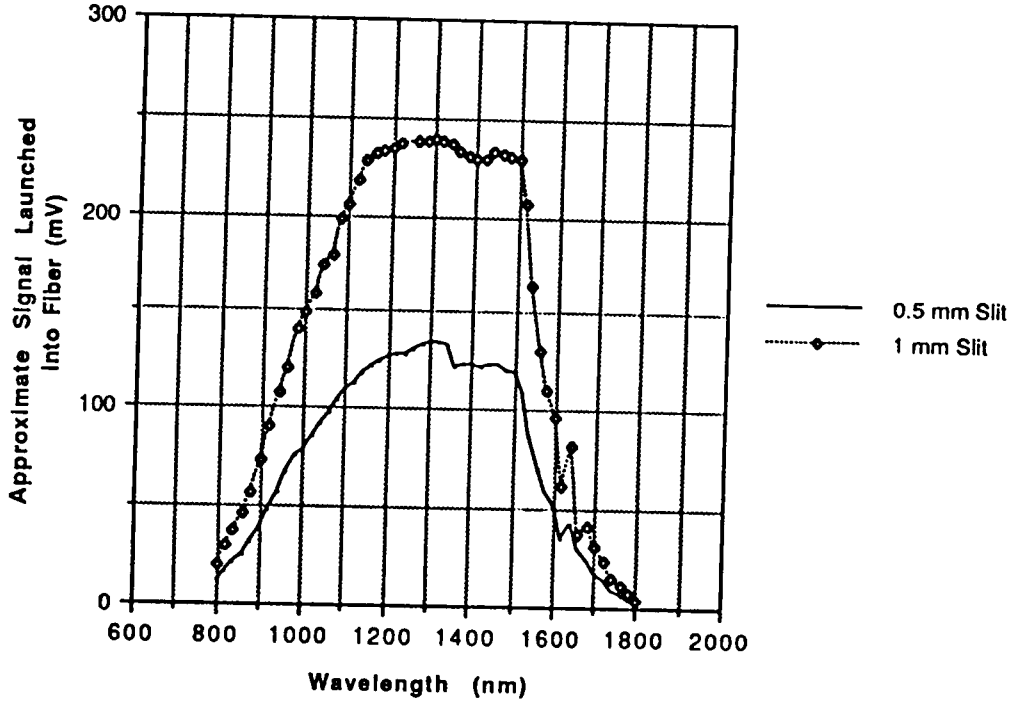

Figure 38. Signal Detected Out of 1 Meter Si Fiber by the Lock-In Amp

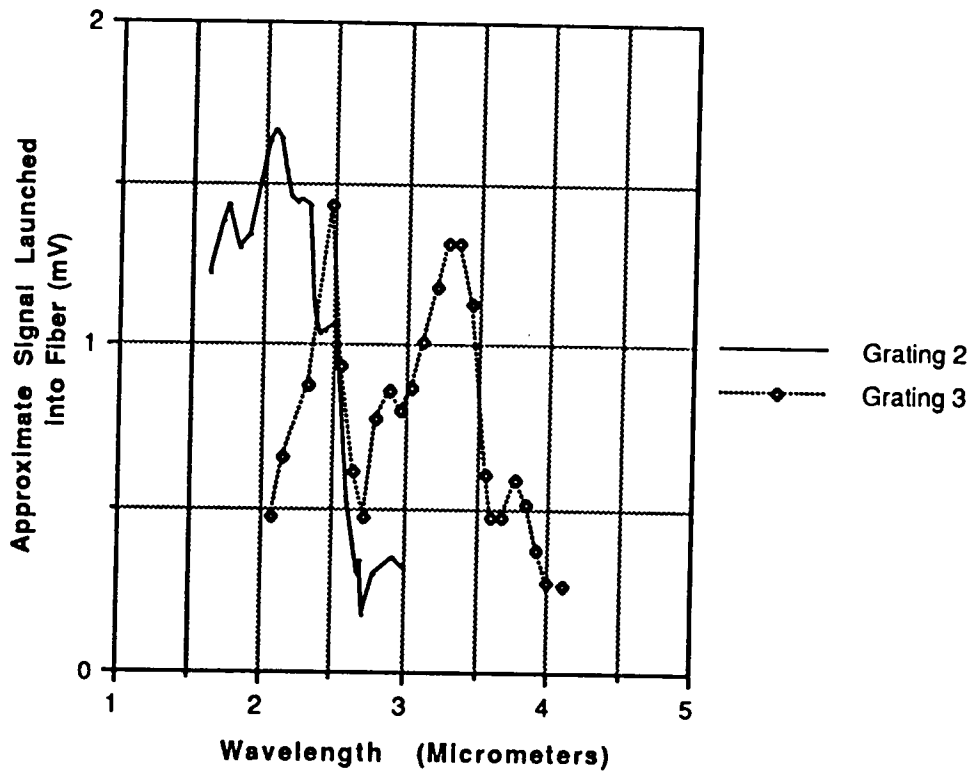

Figure 39. Signal Detected Out of 1 Meter ZrF_4 Fiber by the Lock-In Amp

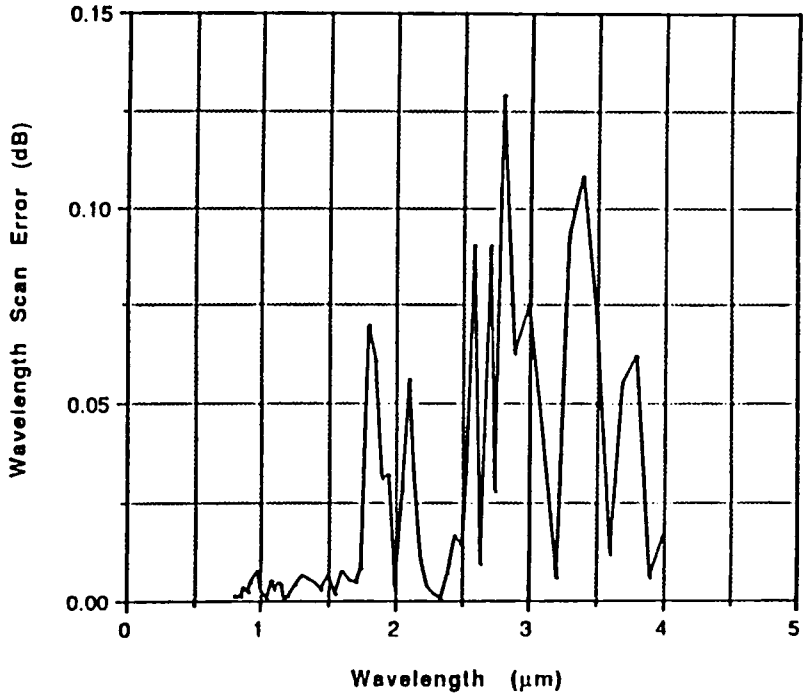

Figure 40. Wavelength Scan Error

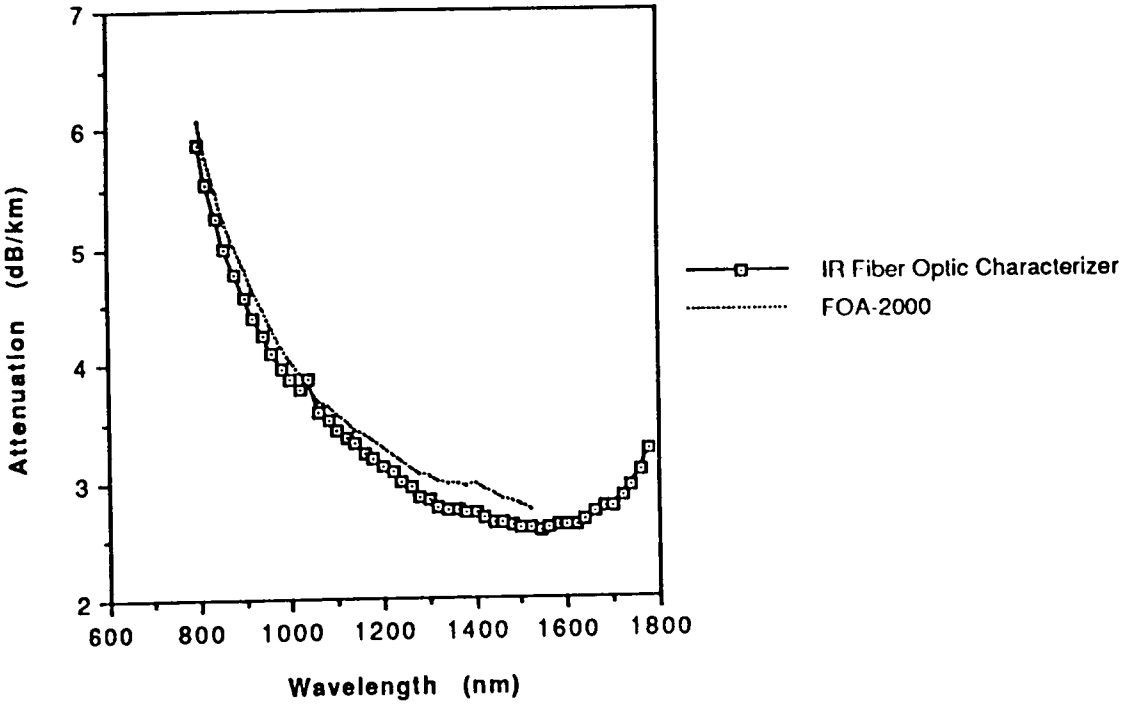

Figure 41. Spectral Attenuation Comparison Between the Two Measurement Systems

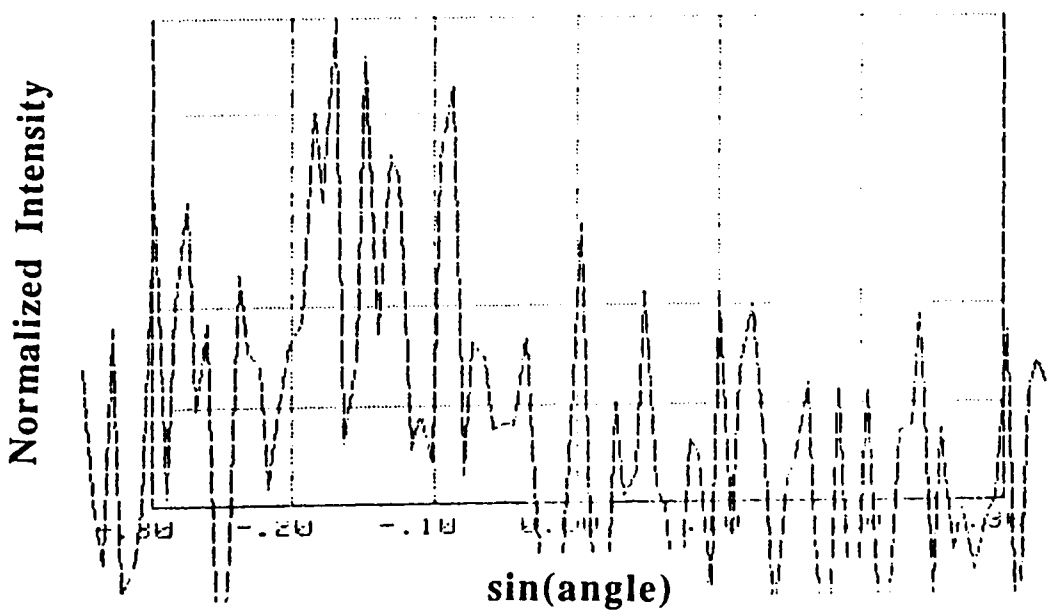

Figure 42. Far Field Scan Using the Pinhole Aperture on the IR Fiber Characterizer

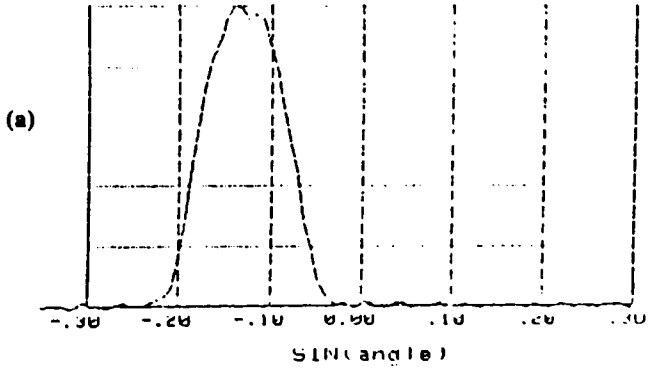

Numerical Aperture - .084

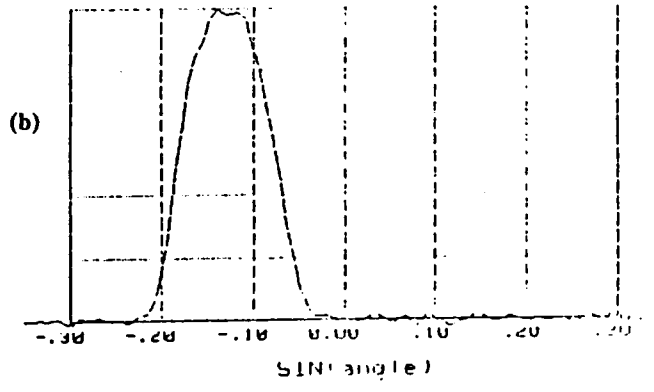

Numerical Aperture - .085

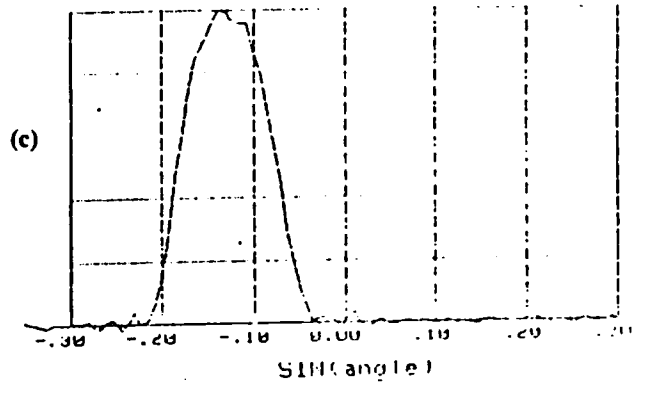

Numerical Aperture - .084

Figure 43. NA Measurement Results Using the Knife Edge on the IR Fiber Characterizer

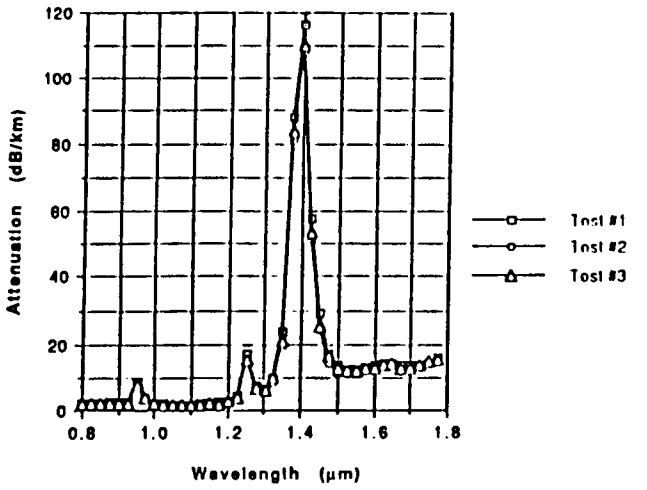

(a)

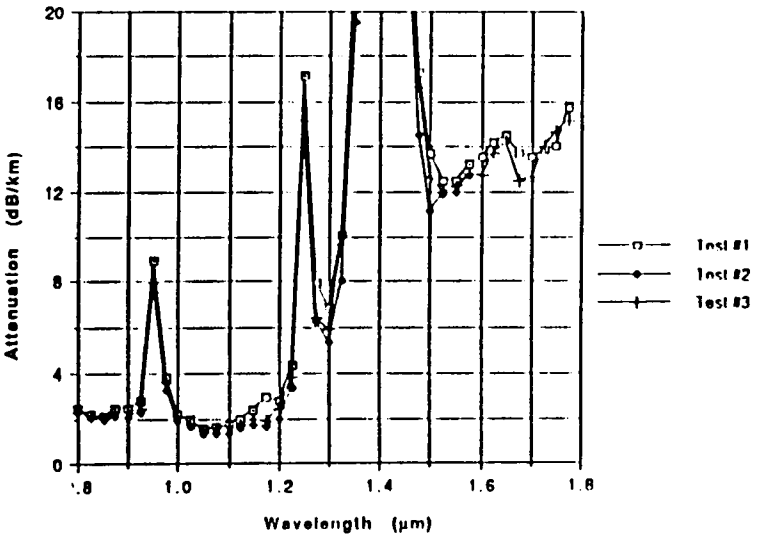

(b)

Figure 44. DMA Repeatability Test (a) Full Scale (b) Reduced Scale

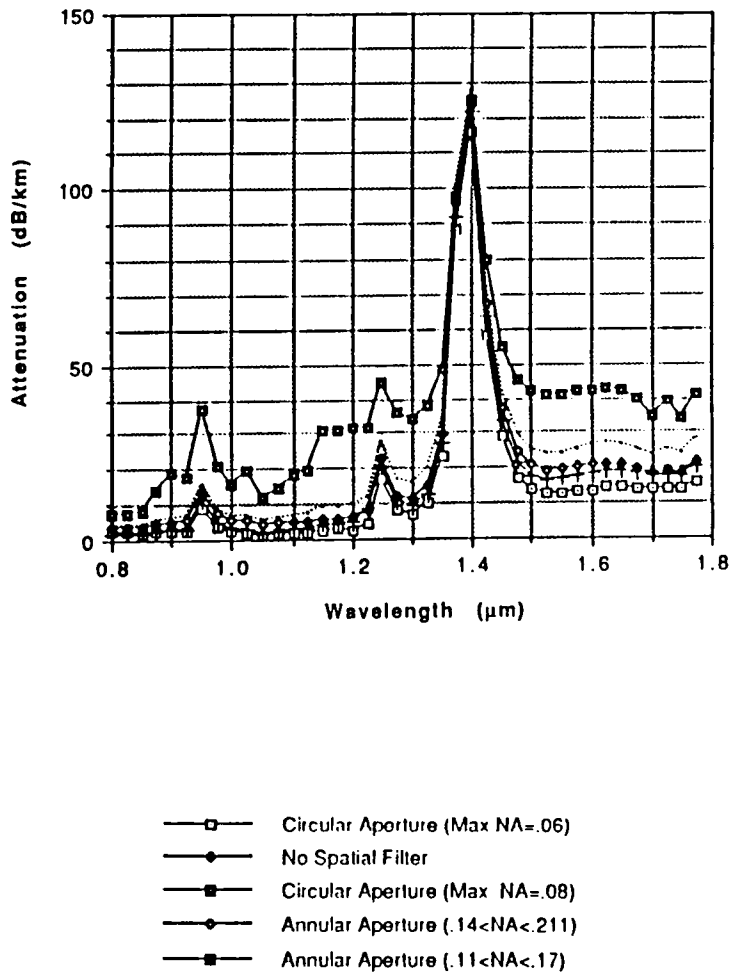

Figure 45. Differential Modal Attenuation Performed Using Several Spatial Filters

7.0 Future Directions & Conclusion

7.1 Future Direction

The automated infrared fiber optic cable characterizer did not effectively perform all the measurement routines. Low power levels from the monochromator limited the dynamic range of the system. Far field scan at 1.55 μm or 2.55 μm using a pinhole was not possible because of the low level of power launched into the fiber. Accurate spectral attenuation measurements for the higher wavelength will also be difficult to obtain because of the low signal levels launched into the fiber. Differential modal attenuation measurement is hindered by the low level of power launched into the fiber when using the spatial filter and launch spot restrictor. A more powerful incandescent source such as a high temperature blackbody may help solve the problem of low monochromator power output. When solid state LEDs are available at 2.55 μm, they can be used as sources for the far field scan and the differential modal attenuation measurements.

A restricted spot size of approximately 35 μm or 1/3 the fiber core diameter is required

when performing differential modal attenuation measurements. The chromatic aberration software for the infrared lenses must be perfected before this restricted spot size on the fiber is obtained over the measurement wavelength interval. Future automated fiber optic characterizers can employ paraboloidal mirrors instead of dielectric lenses to avoid chromatic aberration problems. Other improvements in the system may include a shield for the detectors to reduce stray light from entering. A monochromator with more precise mechanical movements can be employed to reduce the wavelength scan errors.

7.2 Conclusion

The hardware design of an automated IR fiber optic characterizer was presented in this thesis. A description of the design approach and components used on the system was presented. A discussion of the theories associated with spectral attenuation, differential modal attenuation, and far field scanning was addressed.

An IR fiber optic characterizer was constructed and tested. Not all measurement requirements of the system were met but the information in this thesis can help future measurement system designers.

References

1. P. Henry, R. Linke, and A. Gnauck, *Optical Fiber Telecomunication 2*, Academic Press, New York, 1988, p 796-803.

2. G. Sigal and D. C. Tran, "Ultra Low Loss Optical Fibers: An Overview," *Infrared Optical Materials and Fibers 3*, Proc. SPIE 484, p 2-6, 1984.

3. P. France, S. Carter, M. Moore, J. Williams, and C. Day, "Properties of Fluorozirconate Fibers for Application in the 0.5 to 4.5 μm Region," *Infrared Optical Materials and Fibers 5*, Proc. SPIE 843, p 56 1987.

4. K. Ohsawa and T. Shibata, "Preparation and Characterization of ZrF_4 - BaF_2 - LaF_3 -NaF - AlF_3 Glass Optical Fibers," *Journal of Lightwave Technology*, Vol. LT-2, No. 5, p 602-606, October, 1984.

5. D. C. Tran, G. H. Sigel, and B. Bendow, "Heavy Metal Fluoride Glasses and Fibers: A Review," Journal of Lightwave Technology, Vol. LT-2, No. 5, October, 1984.

6. S. Sakaguchi and S. Takahashi, "Low-Loss Fluoride Optical Fibers for MidinfraredOptical Communication," Journal of Lightwave Technology, Vol. LT-5, No. 9, September, 1987.

7. A. L. Mathews, *Application of Infrared Fibers in Temperature Sensing*, MSEE Thesis, p 38, Virginia Polytechnic Institute and State University, 1988.

8. *FOA-2000 Operator's Manual*, Photon Kinetics Incorporated, Beaverton, OR, 1986.

9. P. Klocek, "Theoretical Overview of Limitation of Light Propagation in Infrared Optical Fibers," *Infrared Optical Materials and Fibers 3*, Proc. SPIE 484, p 14-17, 1984.

10. H. Iwasaki, "Development of IR Optical Fibers in Japan," *Infrared Optical Materials and Fibers 4*, Proc. SPIE 618, p 2-9, 1986.

11. K. Nassau, M. E. Lines, "Calculation of scattering and other parameters for ultra low loss optical fibers," Infrared OpticalMaterials and Fibers 3, Proc. SPIE 484, p 7-13, 1984.

12. *Oriel Volume 2*, Oriel Corporation, Stratford, CT, 1987.

13. *Oriel Volume 3*, Oriel Corporation, Stratford, CT, 1989.

14. D. Marcuse, *Principles of Optical Fiber Measurements*, Academic Press, New York, 1981.

15. R. D. Hudson, *Infrared Systems Engineering*, John Wiley & Son Inc., New York, 1969.

16. W. E. Forsythe and E. Q. Adams, "Radiating Characteristics of Tungsten and Tungsten Lamps," *Journal of the Optical Society of America*, Vol. 35, p 109, 1944.

17. K. Harding, "Evaluation of Nernst Glower for 1 to 4 micron operation," *Memorandum D-80-151*, Dayton, OH, 1980.

18. *Blackbody Sources*, Electro Optical Industries Inc., Santa Barbara, CA, 1988.

19. P. W. France, M. C. Brierley, S. F. Carter, M. W. Moore, and J. R. Williams, "Fluoride Fiber Lasers for sources over the wavelength range 1 to 3 μm," *Infrared Fiber Optics*, SPIE 1048,p 124-128, 1989.

20. *Ushio Halogen Lamps Technical Specifications*, Ushio America Inc., Torrance, CA, 1988.

21. *Jarrell-Ash Monospect 27 Monochromator*, Allied Analytical Systems, Waltham, MA, 1988.

22. *Step Motor 39 Series*, Shinano Kensni Corp., Nagaho-Ken, Japan, 1986.

23. S. Musikant, *Optical Materials*, Marcel Dekker Inc., New York, 1985.

24. *Off-Axis Paraboloid Mirrors*, DimondElectro-Optics Inc.,Wilmington, MA, 1988.

25. *Optics Guide 4*, Melles Griot Corp., Irvine, CA, 1988.

26. W. T. Welford, Aberations of Optical Systems, Adam Hilger Ltd., Bristol, England, 1986.

27. *RCA Electro - Optics Handbook*, Commercial Engineering, Harrison, NJ, 1979.

28. Preliminary 1988 Detector Catalog, Infrared Associates Inc., Cranbury, NJ, 1988.

29. R. Olshansky and S. M. Oaks, "Differential Mode Attenuation measurements in Graded - Index Fibers," *Applied Optics*, Vol. 17, No. 11, 1978.

30. A. Safaai- Jazi, *Optical Waveguide Theory* (EE:5980 Class Notes), Virginia Polytechnic Institute and State University, Department of Electrical Engineering, Spring Semester, 1989.

31. G. Keiser, *Optical Fiber Communication*, McGraw - Hill, New York, 1983.

32. L. Jeunhomme and J. P. Pocholle, "Measurement of the Numerical Aperture of a Step Index Optical Fibre," *Electronics Letters*, Vol. 12, No. 3, 1976.

33. *Output Farfield Radiation Pattern Measurement*, Electronics Industries Association, Wasington D. C., 1988.

34. B. Bassin, *Lens Specifications* , Infrared Optics Inc., Farmingdale, NY, 1989.

35. R. Kinglake, *Lens Design Fundamentals,* Academic Press, New York, 1978.

36. L. Jeunhomme, "Experimental Determination of the Radiation Pattern of Optical Fibers," *Optical Communications*, Vol. 12, No. 25, 1974.

37. D, Gloge, "Optical power Flow in Multimode Fibers," *The Bell System Technical Journal*, Vol. 51, No. 8, p 1767-1783, 1972.

38. *Mode Field Diameter of Single-Mode Optical Fiber by Knife-Edge Scanning in the Far Field*, Electronics Industries Association, Washington D.C., 1988.

The vita has been removed from the scanned document